Rubber Elasticity of Polymer Networks in Explicitly non-Gaussian States. Statistical Mechanics and LF-NMR Inquiry in Hydrogel Systems.

Stefano A. Mezzasalma[a,b], Michela Abrami[c], Gabriele Grassi[d] and Mario Grassi[c,*]

[a]*Ruđer Bošković Institute, Materials Physics Division, Bijeniška cesta 54, 10000 Zagreb, Croatia*

[b]*Lund Institute for advanced Neutron and X-ray Science (LINXS), Lund University, IDEON Building, Delta 5, Scheelevägen 19, 223 70 Lund, Sweden*

[c]*Department of Engineering and Architecture, Trieste University, via Valerio 6, I-34127 Trieste, Italy*

[d]*Department of Life Sciences, Trieste University (Cattinara), Strada di Fiume 447, I-34149 Trieste, Italy*

ARTICLE INFO

Keywords:
rubber-like elasticity
statistical mechanics of polymer networks
non-Gaussian statistics
hydrogel swelling
LF-NMR

ABSTRACT

We present a statistical mechanics theory of rubber-like elasticity in swollen and unswollen polymer networks characterized by explicitly non-Gaussian distribution functions (Laplace's, Cauchy's, and continuous Poisson's in the exponential limit). An important outcome is the derivation of new families of statistical and mechanical laws, including a discussion of energy functions of strain invariants, which are reasonably simple for a model comparison with available data on polymer networks. Accordingly, a theoretical-experimental approach based on LF-NMR was devised to identify the most likely end-to-end length distribution in an arbitrary network. When this strategy is applied to agar 1 %, alginate 1 %, and scleroglucan 2 % hydrogels, it turns out that the end-to-end distribution should be never regarded as Gaussian even if, as in agar and scleroglucan systems, the normal statistics is the best among those here regarded. Remarkably, Poisson's distribution is proved instead to be the most realistic for the alginate hydrogel.

1. Introduction

Rubber elasticity theory had probably the most enduring history in all of polymer disciplines, displaying a remarkable size of discrepancies with experimental data which were intensively and contradictorily debated for decades (see e.g. bibliography in Hild (1998)). The agreement one is usually left with is mainly qualitative and the probability distribution function governing the nascent network, whether it is swollen or unswollen, is generally unknown (Huang, Szleifer and Peppas, 2002). A crucial question, which still remains, is a profound self-consistent description of microscopic chain conformations versus macroscopic network deformations, as the basic properties of deformation processes can only be explained qualitatively by means of topology arguments. Many disputes were on the roles of cross-link junctions, their fluctuations, cooperative movements and constraints they exert on the (first) neighbouring chain conformations (Candau, Bastide and Delsanti, 1982) and any relevant steric interaction, specially entanglements and various types of network defects, like physical and intramolecular crosslinks (Gedde, 1995). Topological constraints are not ascribable to chemical cross-links, they are very heterogeneous, act as interchain effects almost continuously along the chain and ultimately interplay with elastic and osmotic forces (Priss, 1981; Panyukov and Rabin, 1996). Entangled points, in particular, are temporary and of short duration (Hild, 1998). Mullins' early hypothesis, to deal with an apparent crosslink number summing chemical junctions and physical entanglements, was afterwards denied (Gedde, 1995).

Over the years polymer scientists complemented and/or corrected the classical theories by more realistic mechanisms (Priss, 1981). Gaussian mean-field assumptions, in fact, are anyway restrictive (e.g. small elongations, networks prepared by coalescing concentrated solutions with compressed or weakly stretched chains, etc.) and, normally, better tolerated in the dry state, which is representative of dense neutral polymer systems where excluded volumes screen out. On the other hand, swollen networks in good solvents are notoriously non-Gaussian, the most effective, yet elegant analysis, being still given by de Gennes' scaling theory, furnishing a universal description in terms of blob correlations (de Gennes, 1979). Between dilute and Gaussian regimes, chain conformations behave as a random walk of blobs

Corresponding Author; e-mail: Mario.Grassi@dia.units.it
ORCID(s):

with correlation length equal to the average mesh size of semidilute solutions (see e.g. Mezzasalma (2008)). The c^* theorem, however, only holds in networks with almost regular topology and synthesized at the overlap threshold between dilute and semidilute regimes (Panyukov, 1990), while real swelling phenomena are affected by topological disorder and inhomogeneities (entanglements, dangling ends, closed loops, crosslink reactions), trapped in the preparation process, by heterogeneous fluctuations in the cross-link density, increasing beyond the thermodynamic values, and by geometric effects (Johner, Vilgis and Joanny; Panyukov, 1989, 1990; Mezzasalma, 2001). Cross-link density seems itself to be an ill-defined variable that, particularly in highly cross-linked states, strongly depends on the adopted model (Valentín, Carretero-González, Mora-Barrantes, Chassé and Saalwächter, 2008). Even to define a consistent measure for polymer volumes is not an immediate task, as the average network energy seems to scale with anomalous exponents that are incompatible with mean-field approaches (Hadizadeh, Linhananta and Plotkin, 2011).

Besides statistical mechanics of networks, their topology and continuum mechanics, a second analysis level focuses on chain conformations and chemical structure, like the quite recent inquiries into segmental orders show. In short, vector order parameters, inaccessible to NMR, relates to the residual chain orientation, while tensor parameters from multi-quantum NMR measurements characterize the fluctuation extents in segment orientations. The true network elasticity follows in fact from the actual conformation space made available to chain portions, i.e. from the excursion of individual segment orientations. The narrow dynamic profile that comes from local NMR measurements in elastomers thus suggests that the single chain description relying on a purely affine model should fail (Saalwächter and Sommer, 2007). Alongside Edwards' second-moment tensor parameter, of flexible excluded-volume polymers in a weakly good solvent, displays a inhomogeneous distribution decaying along the chain, with lower segmental orders than in Gaussian statistics (Usatenko and Sommer, 2008). End-linked mono- and bi-modal networks were also studied by means of Monte Carlo bond-fluctuation simulations. The vector order parameter of longer chains was twice as large as in Gaussian systems, the shorter ones displaying a much lower value than expected (Sommer, J. -U. and Saalwächter, K., 2005). Such discrepancies suggest that interchain effects may influence the bond orientation even in concentrated states, where Gaussian statistics should be expected (de Gennes, 1979).

Motivated by this challenging picture, an alternative view is proposed here to formalize the effect of explicitly non-Gaussian states in the distribution function of polymer networks, and then to devise an NMR-based discrimination criterion. Experimentally, despite the large number of characterization techniques for cross-linked networks (such as inverse gas chromatography, neutron scattering, osmometry, dielectric and mechanical analysis, see e.g. references in (Valentín et al., 2008)), the most exploited remain NMR spectroscopy and equilibrium swelling. Attention will be paid here to hydrogel behaviors, either interesting from the fundamental point of view, where distinct elasticity regimes can occur according to polymer dilution (Gundogan, Okay and Oppermann, 2004), or for their notable large-strain features (Gong, Katsuyama, Kurokawa and Osada, 2003; Webber, Creton, Brown and Gong, 2007). Theoretically, the present work puts forward an intermediate model placing itself between the refinement of affine versus phantom theories and the analysis of Gaussian versus non-Gaussian effects.

It is known in fact that two milestones of polymer elasticity theory, both based on (unentangled) Gaussian statistics in an infinite network with no loose chain ends, are the 'classical' junction affine and phantom models, related respectively to the uppermost and lowermost chain deformation limits. The elastic response of rubber networks and swollen systems is generally believed to be intermediate between such two extremes, with an uncertainty on cross-link densities of $\approx 40\%$ the phantom-like value (Valentín et al., 2008). In the former, macroscopic and microscopic deformations are assumed to be practically the same, cross-links being fixed in space to positions imposed by the specimen deformation ratio (α). Junction points in James and Guth's phantom model are instead unrestricted, only a small fraction of them being anchored to the boundary surface (Burak Erman, 1989) and chains in between being only constrained to the forces they are subjected to (Flory and Erman, 1982). Crosslinks are modeled by holonomic constraints (Eichinger, 2015) to move affinely around the average positions prescribed by the macroscopic deformation (Gedde, 1995) and are roughly confined to the root mean square end-to-end distance of a network strand (Gottlieb, 1982), i.e. much smaller than the contour chain length but large enough to allow an overwhelming majority of possible conformations (Gedde, 1995). Fluctuations in this model are taken to be strain-independent, developing asymmetrically in deformed states and reducing the strain below the value set by the experiment (Mark, 1992). One is therefore left with a chain functionality-dependent (f) non-affine transformation of instantaneous end-to-end distance and of mean gyration radius of elastic chains (Candau et al., 1982). Microscopic deformations, especially in stiff or semiflexible chains, should become non-affine below a certain length scale and/or above a certain deformation degree (Basu, Wen, Mao, Lubensky, Janmey and Yodh, 2011; Curro and Mark, 1984).

Despite the affine hypothesis was afterwards discarded for the phantom network, the latter turns out to be still inaccu-

rate (Hild, 1998). Furthermore, as the two theories rely on a number of alike assumptions (e.g. individual chain models with only intramolecular effects and the same network forces (Gedde, 1995), chain vector distribution in undeformed network equal to the single chain's in uncrosslinked bulk Burak Erman (1989)), it is no surprise that both free energy and stress-strain equations are similar, to the point of concluding that no essential difference between James-Guth's and Flory-Wall's theories would take place (Eichinger, 2015). More rigorous constrained junction theories (Ronchi-Allegra's, Flory-Erman's, Edward's tube, non-affine and slip-link models Ronca and Allegra (1975); R.C., M., S.F. and M. (1981); Flory and Erman (1982); Erman and Flory (1982a); Mergell and Everaers (2001); Rubinstein and Panyukov (2002); Erman (2010)) describe in detail the dependence of fluctuations on deformations to get the excess free energy in comparison to classical (phantom) theories, where elasticity is only affected by network connectivity, and time averages only transform with the macroscopic deformation. Overall, they were able to explain stress-strain data in intermediate extension ranges (say, up to $\alpha \approx 2$), when fluctuations are far from being suppressed and deformation makes cross-links more mobile (Gedde, 1995). On the contrary, for a network subject to small deformations or high junction interpenetration, crosslinks are strongly hindered, their instantaneous position well approximating the affinity condition to the external strain (Gottlieb, 1982; Ngai and Roland, 1994).

As the role of chain vector distributions is exceptionally important here, a number of non-Gaussian network models were proposed to refine the theoretical predictions (see e.g. the overview in (Elías-Zúñiga, 2006)). The Gaussian distribution only corresponds to the first linear term in the force-extension relation for a single polymer chain (Treloar, 1973), it neither matches (very) short chains nor the limit of high enough elongations (e.g. (Gedde, 1995) $\alpha > 3$), when the mechanical response displays marked upturns (Burak Erman, 1989; Elías-Zúñiga and Beatty, 2002). A problem is it doesn't fall to zero at the contour length scale (Treloar, 1973), though an explanation in terms of limited extensibility then was discredited. Experimental workers detected modulus upturns in natural rubbers only in networks undergoing strain-induced crystallization at high elongations (Mark, 1992). Another issue is in the monomer number between two cross-links, often ≤ 100, chains being not long enough to be regarded in the Gaussian limit (Huang et al., 2002). Polymer scientists were traditionally employing analytical and semi-heuristic models, with expanded or perturbed Gaussian distributions (e.g. Fixman and Alben (1973)), or combining finite chain extensibility with entanglement effects (e.g. tube models Erman (2010)), rotational isomeric state models (Mark and Curro, 1983) and computations of short-chain distributions (Curro and Mark, 1984). Again, it should be remarked that the agreement achieved by numerical simulations of non-Gaussian systems may be only qualitative (Menduina, Freire, Llorente and Vilgis, 1986).

To the best of the authors' knowledge, this is the first time a non-Gaussian statistics is used *in explicit form* in a rubber-like elasticity theory. In Treloar's words (Treloar, 1975) "Unfortunately the attempt to replace the Gaussian statistical theory by a more exact treatment involves a considerable sacrifice of both simplicity and generality. ... The treatment of this problem in a rigorous manner presents formidable mathematical difficulties." However, the final equations we obtain are quite simple and lend themselves to a prompt check. To do so, a strategy relying on Low-Field NMR is proposed to pseudo-experimentally infer the end-to-end distribution in real hydrogels. In this paper, we applied it to alginate, agar and scleroglucan hydrogels, that is, three examples of amply used materials for biomedical use and drug release (Matricardi, Alhaique and Coviello, 2016). It is important to remind the non-Gaussian character we refer to is not associated to a polymeric network approaching its extensibility limit (upon swelling), a condition that requires adopting the inverse Langevin's function (or more conveniently some approximation of it, as proposed by Warner (Bird, Armstrong and Hassager, 1990)) to model the swelling equilibrium (Coviello, Grassi, Rambone and Alhaique, 2001). Our focus on the contrary is on the possibility that, just after crosslinking as well, the end-to-end chain distribution function does not follow a Gaussian behavior, this being still one of the main limitations of Flory's theory, as it was further emphasized quite recently (Richbourg and Peppas, 2020).

The distributions chosen here as candidates for the network states of interest are Laplace's, Cauchy's and Poisson's. They have the two-fold purpose of formally mimicking the normal law but deviating from it to a quantitative extent that can be regarded not only perturbative (see next Fig. 1). The former, in fact, was formulated by Laplace some years before the 'second law of errors' (i.e. the Gaussian) and takes place in a wealthy of stochastic applications, like modeling sizes of sand particles, diamonds and beans (Kotz, Kozubowski and Podgorski, 2001). From a technical viewpoint, in a similar way as to Lindeberg & Feller's central limit theorem (Feller, 1991), it is shown that a suitably normalized geometric sum of independent random variables converges in law to Laplace's even though they are not identically distributed (Toda, 2011). Poisson's law represents the asymptotic regime of phenomena like waiting times, extremes, quasi-stationary distributions and rare events (Peköz and Röllin, 2011). Mathematically, this turned out to be the toughest distribution, but here it was also necessary to complete and discuss in more detail the statistical mechanics picture raised by Laplace's law. Getting explicit bounds on the error of the exponential limit may be notably difficult

as well (Aldous, 1989). In between, the broad-tailed Cauchy's law (or Cauchy & Lorentz') is part of the extended family of Lévy or stable distributions. It doesn't possess a generating function, thence is an exception to the wealthy of laws belonging to the attraction domain of the central limit theorem, which only requires the first two moments to be finite. In spite of this anomaly, it keeps a central place in a number of physical and chemical topics, such as Ornstein & Zernike's theory of critical opalescence (Ornstein and Zernike, 1914), the lifetime broadening of spectral lines (Thorne, 1988) and Lorentz' model for the complex electric permittivity (Fox, 2001).
As a short outline, sections (2-4) of the paper deal with the statistical mechanics derivation of the theory whereas, in the second part, the focus is shifted on a Low-Field NMR-based approach for deriving the realistic end-to-end distribution function in hydrogels. An analysis of the model outputs in light of experimental data is conducted in section (6). In developing the theory, instead, we will stick to the conceptual route (and notations) devised by Flory in Chapters (X-XI) of his seminal book (Flory, 1953), aiming to a generalization to polymer networks which are not ideal.

2. Network Entropy Function

2.1. General Formulation and Link to Mechanics

The analysis hereby presented is in line to the statistical mechanics tradition developed from the beginning until recently, which assumes the work of deformation (i.e. the strain energy density U (Dietmar and Thomas, 2011)) to be proportional to the change of entropy (S) on stretching the chains from the undeformed state. For an isotropic and incompressible hyperelastic material, the principal Cauchy stress components (σ_k) then stem from U as (Beatty, 2003):

$$\sigma_k = \alpha_k \frac{dU}{d\alpha_k} + p \qquad \text{(no sum over repeated indices)} \tag{1}$$

α_k here denoting the principal elongation stretches (often also referred to as λ_k) and U being symmetric functions of α_k. The hydrostatic pressure term (p) comes from the incompressibility or constant volume condition (i.e. the Jacobian $J = 1$ in the next Eq. 7), since it is no longer determined by the strain energy density and needs to be added explicitly as a constraint on U. Evidently, any difference between two principal stresses:

$$\sigma_j - \sigma_i = \alpha_j \frac{dU}{d\alpha_j} - \alpha_i \frac{dU}{d\alpha_i} \tag{2}$$

cancels out the effect of p. Eq. (2) then may undergo the fundamental conditions of mechanics, such as Baker-Ericksen inequalities, $(\alpha_j - \alpha_i)(\sigma_j - \sigma_i) > 0$ $(j \neq i)$, postulating the larger principal stress to always establish along the direction of the larger principal stretch (Baker and Ericksen, 1954; Wilber and Criscione, 2005). A fascinating aspect of rubber elasticity is that a complex deformation curve can be rebuilt up by means of a mesoscopic analysis, in which the random arrangement of monomer units (in an elastomer or in a gel) is modelled by a given statistical mechanics approach. The relationship between randomness and mechanical response ultimately form the subject of the present investigation, the entropy function representing the key property that needs to be in focus. Ignoring any enthalpic contribution, as usual in these cases, the statistical thermodynamics function connecting Eq. (1) to the thermally driven state of a random network is Helmholtz free energy $F = -TS$ (T = absolute temperature) per unit referential volume (V_0). If entropy refers to a single chain, the number density of crosslinked strands (e.g. n^*) can be employed to tackle a polymer network (Rubinstein and Colby, 2003; Huang, 2014; Arruda and Boyce, 1993):

$$U\left(\{\alpha_k\}\right) = \frac{F}{V_0}\left(\{\alpha_k\}\right) = -n^* T S\left(\{\alpha_k\}\right) \tag{3}$$

Contributions from interchain interactions are basically thermodynamic and not expected to take any role in elastic free energy calculations. Therefore, despite the main emphasis is given here to the elastic part of the entropy function, the reader may remember that any statistical point of view on the network will correspond to a given strain energy density (for a survey of phenomenological constitutive equations in rubber-like materials see e.g. Destrade, Saccomandi and Sgura (2017); Puglisi and Saccomandi (2016)). When non-negligible heat transfers may develop, F is ceasing however to be fully representative of the network behavior.
With this in mind, our starting point is Flory's entropy decomposition into a configuration and an ideal gas contributions, that is, in Boltzmann's constant unit (k_B):

$$\ln \Omega = \ln \Omega_1 + \ln \Omega_2 \tag{4}$$

where Ω and Ω_k denote the respective partition functions (sums over microstates) with $S = \ln\Omega$ and $S_k = \ln\Omega_k$. What will matter is clearly the entropy change upon deformation, the difference ΔS between the initial and final states. In what follows such two terms ($\Omega_{1,2}$) will be given a separate account, making the customary assumption to deal with different overlaps of conformational domains, extensibility, steric and connectivity effects (Hermans, 1962) in terms of three explicitly non-Gaussian statistics. While the Gaussian distribution alone cannot account for conformational differences between unlike types of polymeric chains, it is known that stress-strain behaviors can be affected by the chain structure even in very small deformation limits (Mark and Curro, 1983). Swelling networks then can display large macroscopic deformation with no meaningful change of chain dimensions, this behavior being tough to be translated in the language of classical theories (Candau et al., 1982).

Note again that, as Flory-Rehner's hypothesis assumes the free energy to be additive, Eq. (4) doesn't include interaction and liquid-like terms, elastic contributions are the only ones depending on deformation (Flory and Rehner, 1943a). The independence of spatial configurations of intermolecular interactions was thoroughly tested, especially by neutron scattering experiments in undiluted amorphous polymers and classical rubbers, where steric interactions are short-ranged and force fields are weak (see e.g. (Mark, 1992) and references therein) but was afterwards criticized by a number of authors (Ball and Edwards, 1980; Edwards and Vilgis, 1988; Sommer, Vilgis and Heinrich, 1994; Vilgis and Wilder, 1998; Baek and Srinivasa, 2004). However, while an inquiry into Flory-Renher's hypothesis falls outside the aim of the present study, classical or perturbed rubber elasticity models still find a wealthy of applications, including the hydrogel systems that will form the subjects of our investigation (Koetting, Peters, Steichen and Peppas, 2015; Chan and Neufeld, 2009). Also the thorny relation between statistical mechanics and continuum theory (Eichinger, 2015) as well as explicit concentration effects on fluctuations of cross-link points (Candau et al., 1982) won't be accounted here for. Finally, in the spirit of a milestone work on non-Gaussian effects (James and Guth, 1943; Treloar, 1973), the affinity assumption will be retained in the next elaboration of extension-force relationships (James and Guth, 1943; Treloar, 1973). The perfect gas entropy term in Eq. (4) will then be generalized in compliance with the conformational statistics, yielding a hybrid model that is able to retrieve the phantom limit behavior by means of local or microscopic elasticity constraints.

In conclusion to this section, to further clarify our central aim, this work stems from a doubt that may have often been quelled over the years. Is it permissible that, for some micro- or meso-structural reasons, presumably related to physical chemistry or topology of monomer strands, the architecture of a polymeric network may be (explicitly) non-Gaussian also in undeformed conditions ? Theoretical approaches generally involving the inverse Langevin function (e.g. eight-chain and full network models) have already been known for decades to catch the stress-strain curve at large deformations due to the finite extensibility of polymer chains (Wu and van der Giessen, 1992; Arruda and Boyce, 1993; Bechir, Chevalier and Idjeri, 2010). Our point of view here is rather different. What would happen to the mechanical response once the Gaussian hypothesis were somehow relaxed, or even dropped, near enough the low stretch regime ? The present exploratory inquiry tries to open up a debate on this quest, nonetheless taking care to provide an adequate theoretical background and a thorough experimental verification to the ideas hereby presented.

2.2. Configuration Term

The first entropic term quantifies the statistical mechanics effects of the distribution function for the end-to-end chain displacement in the deformed state, $W = W(\mathbf{r})$:

$$\frac{1}{\nu}\ln\Omega_1 = \ln \mathrm{J} + \int_{\mathfrak{R}^3} W(\mathbf{R}) \ln\frac{W(\mathbf{r})}{W(\mathbf{R})}\, d\mathbf{R} \tag{5}$$

where ν is the number of crosslinked strands, taken to be homogeneously distributed in the sample (Beatty, 2003). By this density of probability, the local chain strain at the mesoscopic level is transferred to the macroscopic scale of the contiguous particle-system (i.e. the continuum) hosting the process. For an undeformed system, undergoing a material point transformation in the stretched state, $\mathbf{R} \to \mathbf{r}$, the scalar quantity:

$$\mathrm{J} = \left\| \frac{\partial \mathbf{r}}{\partial \mathbf{R}} \right\| \tag{6}$$

is the Jacobian determinant of the deformation gradient $\mathbf{F} = (\partial\mathbf{r}/\partial\mathbf{R})$ (or, simply, the gradient of $\mathbf{r}$). This mapping is generally assumed to be a one-to-one and smooth function (for a rigorous introduction to these concepts, see e.g. Beatty (1987)). The image ($d\mathbf{r}$) of a tangent element to an undeformed material line ($d\mathbf{R}$), pointing out the separation vector

between two materials points in the reference state, then is set univocally by $d\mathbf{r} = \mathbf{F}d\mathbf{R}$, irrespective of the deformation gradient decomposition into pure stretch and rotation tensors. The square of the local change in separation distances stems from the related right and left Cauchy-Green's deformation tensors, e.g. $d\mathbf{r}^2 = d\mathbf{R}\cdot\mathbf{C}\cdot d\mathbf{R}$ with $\mathbf{C} = \mathbf{F}^T\mathbf{F}$ (right tensor). We won't enter details of deformation tensors in the following as, to our purposes, it will suffice to represent undeformed and stretched configurations in Cartesian coordinates (Flory, 1953) with respect to an orthonormal basis $\{\mathbf{e}_k\}$, and set $X_i = x_i/\alpha_i$, i.e.:

$$\mathrm{J} \;=\; \prod_i \alpha_i \;\;, \tag{7}$$

$x_i = \mathbf{e}_i\cdot\mathbf{r}$ being the transformed coordinates of $X_i = \mathbf{e}_i\cdot\mathbf{R}$, while $\alpha_i \equiv \alpha_x, \alpha_y, \alpha_z$ are the positive elongation coefficients or extension ratios, characterizing a pure homogeneous deformation gradient.
The term Ω_1 is only affected by the statistics of polymer molecules forming the elastic medium. In order to detect some meaningful variation from classical results, the conditions of the central limit theorem should be somehow violated. It is well known, in fact, that the Gaussian distribution, $W_n(\mathbf{r}) = (\beta/\sqrt{\pi})^3\exp(-\beta^2\mathbf{r}^2)$, leads to:

$$\tfrac{1}{\nu}\ln\Omega_{1n} \;=\; -\,\tfrac{1}{2}\sum_i \alpha_i^2 \;+\; \tfrac{3}{2} \;+\; \ln\mathrm{J} \tag{8}$$

in which the constant $\beta^2 = 3/(2Nl^2)$ is only influenced by intrinsic polymer properties such as Kuhn's segment length l and monomer unit number N (i.e. the chain displacement length). The above quadratic expression in α_i may be deemed as the signature of the ideal behavior. Clearly, if the probability density is no longer Gaussian, $\ln\Omega_1/\nu$ could sensibly deviate from Eq. (8). This is shown in Appendices A-B, reporting the calculations for three even and continuous distribution functions that monotonically decrease in $|x_i| \in [0,\infty)$. To this aim, we factorize W with respect to each coordinate:

$$W(\mathbf{r}) \;=\; \prod_i W_i(x_i) \tag{9}$$

and make use of the following property:

$$\int_{\mathfrak{R}^3} W(\mathbf{R})\ln\frac{W(\mathbf{r})}{W(\mathbf{R})}\,d\mathbf{R} \;=\; \mathrm{J}^{-1}\sum_{i\neq r\neq s}\alpha_r\alpha_s\bar{\mathrm{I}}_i \tag{10}$$

with:

$$\bar{\mathrm{I}}_i = \int_{-\infty}^{\infty} W_i(X_i)\ln\frac{W_i(x_i)}{W_i(X_i)}\,dx_i \tag{11}$$

being a reduced configuration integral. Therefore, as:

$$\int_{\mathfrak{R}^3} W(\mathbf{R})\ln\frac{W(\mathbf{r})}{W(\mathbf{R})}\,d\mathbf{R} \;=\; \sum_i \frac{\bar{\mathrm{I}}_i}{\alpha_i} \;\;, \tag{12}$$

one can redefine:

$$\bar{\mathrm{I}}_i(\alpha_i; W_i) \;\equiv\; \int_{-\infty}^{\infty} W_i(X_i)\ln W_i(x_i)\,dx_i + \;\mathrm{c}_i\alpha_i \tag{13}$$

$$\mathrm{c}_i \equiv \;-\int_{-\infty}^{\infty} W_i(s)\ln W_i(s)\,ds \;\;, \tag{14}$$

and observe the most important (elastic) contribution to $S_1 = \ln\Omega_1$, the one genuinely linked to the deformation, arises from the first term on the right side of:

$$\int_{\mathfrak{R}^3} W(\mathbf{R})\ln\frac{W(\mathbf{r})}{W(\mathbf{R})}\,d\mathbf{R} \;=\; \sum_i \mathrm{I}_i + \mathrm{c}_i \tag{15}$$

i.e. from the sum of reduced integrals like:

$$\mathrm{I}_i(\alpha_i; W_i) \;=\; \int_{-\infty}^{\infty} W_i(t) \ln W_i(\alpha_i t)\; dt \quad , \tag{16}$$

whereby:

$$\mathrm{I}_i(1; W_i) \;=\; -\,\mathrm{c}_i \tag{17}$$

stands for an entropic constant, representative of the undeformed state. As the mechanical response that will be inquired in an isothermal system stems from entropy variations, whenever the configuration integral is too complicated or does not admit an explicit solution, one may start directly from the derivatives $\partial \mathrm{I}_i / \partial \alpha_i$. Obviously, the values for a Gaussian network:

$$\mathrm{I}_{in} + \;\mathrm{c}_{in} \;=\; -\,\tfrac{1}{2}\left(\alpha_i^2 \;-\; 1\right) \tag{18}$$

are recovered by setting $W_{in} \equiv W_n(x_i)$ in Eq. (15). In the other cases, the first configuration integrals, recalculated in Appendices A-B for three meaningful statistics (Laplace', Cauchy', Poisson's), give us:

$$\tfrac{1}{\nu} \ln \Omega_{1L} \;=\; -\,(\alpha_x + \alpha_y + \alpha_z) \;+\; \ln(\alpha_x \alpha_y \alpha_z) \;+\; 3 \quad \text{(Laplace)} \tag{19}$$

$$\tfrac{1}{\nu} \ln \Omega_{1C} \;=\; -\,\ln(1+\alpha_x)^2 \;-\; \ln(1+\alpha_y)^2 \;-\; \ln(1+\alpha_z)^2 + \;\ln(\alpha_x \alpha_y \alpha_z) \;+\; 6 \ln 2 \quad \text{(Cauchy)} \tag{20}$$

$$\tfrac{1}{\nu} \ln \Omega_{1P} \approx \;\tfrac{1}{\nu} \sum_i \ln \Omega_{i,1P} \qquad \text{(Poisson)} \tag{21}$$

where, in the last equation, the sum:

$$\tfrac{1}{\nu} \ln \Omega_{i,1P} \;=\; -\,(\ln \lambda_i)^2 \alpha_i \;\Xi_{\lambda_i}[1] \;+\; (\ln \alpha_i)(\ln \lambda_i)\; \Xi_{\lambda_i}\left[t^{-1}\right] \;+\; (\ln \lambda_i)\; \Xi_{\lambda_i}\left[t^{-1} \ln \Gamma(\alpha_i t)\right] \;+\; \text{const.} \tag{22}$$

applies to a continuous Poisson's density (Ilienko, 2013) with parameters approaching the exponential regime ($\lambda_i \ll 1$), and:

$$\Xi_\lambda\left[\mathrm{g}\right] \;\equiv\; \int_0^{\infty} \mathrm{g}(t)\; \frac{\lambda^t}{\Gamma(t)}\; dt \tag{23}$$

is a functional based on the gamma function (Γ). A comparison among Eq. (19), Eq. (20) and Eq. (21), which quantify the configuration entropy function per polymer strand S_1 / ν, is reported in the section on results and discussion.

2.3. Perfect Gas Term

We recast here the combinatorial procedure leading to (the controversial) Flory's logarithmic contribution to the total entropy function. Despite James and Guth criticized it harshly, the theoretical view they put forward as an alternative would be devoid of a realistic unstressed state whether a log-term were neglected or absent (Eichinger, 2015; Hild, 1998). Ronca and Allegra made the point it should appear instead in the free energy every time macroscopic deformation and junction fluctuations couple to a non-negligible extent (Ronca and Allegra, 1975).
Second Flory's contribution stems from the likelihood of finding all crosslinked units coupled throughout a network with volume V_0 that deforms to $V = \mathrm{J} V_0$. We may begin from regarding the probability to find any of the (adjacent) ν units in an elementary (small) volume δv, regarded to be intrinsically constant. Adopting the framework of Bernoulli's trials, at a given step m, such a probability can be written as:

$$P_{\nu m} \;=\; \binom{\varphi_{\nu m}}{1} p\; q^{\varphi_{\nu m} - 1} \tag{24}$$

with $\varphi_{\nu m} = \nu - 2m + 1$ and $p = 1 - q = \frac{\delta v}{V}$. As $p \ll 1$, then:

$$P_{\nu m} \approx \varphi_{\nu m} \frac{\delta v}{\mathrm{J}V_0} \tag{25}$$

and the number of states associated with this process in an ideal network is:

$$\Omega_{2n} = \prod_{m=1}^{\frac{\nu}{2}} P_{\nu m} \approx \left(\frac{\nu}{2}\right)! \left(\frac{2\delta v}{\mathrm{J}V_0}\right)^{\frac{\nu}{2}} \tag{26}$$

in which $\left(\frac{\nu}{2}\right)! \equiv (\nu - 1)(\nu - 3) \ldots 1$. The final calculation follows from application of Stirling's formula under $\nu \gg 1$:

$$\frac{1}{\nu} \ln \Omega_{2n} \approx -\frac{1}{2} \ln \mathrm{J} + \text{const.} \tag{27}$$

We note that δv is an indivisible, 'pointwise' volume, totally unaffected by chain configurations near interlinking sites. So long as the experiment is isochoric, Eqn. (27) has no effect. However, based on our strategy to effectively compare different statistics, a generalization of the perfect gas term is necessary to account for the involved probability density at the junction scale, allowing crosslink points to fluctuate accordingly. In the discrete process Ω_2, the functional form $W = W(\mathbf{r})$ thus will be regarded by means of a new perturbation term. Precisely, we reformulate $\delta v/V$ as the likelihood that two network points belong for simplicity to a rectangular neighborhood with volume $\delta V = \prod_i \delta x_i$ $(i = x, y, z)$:

$$p = \prod_i \int_{-\frac{\delta x_i}{2}}^{\frac{\delta x_i}{2}} W_i(u)\, du \tag{28}$$

and factorize it so to separate the contribution connected to δV, which now identifies the new probability to work with $(p \to P)$, from its coordinate-dependent part. Calculus of probability may be framed still in the context of Bernoulli's trials, but this time with P in place of p, and with:

$$\Pi_{\nu m} = \binom{\varphi_{\nu m}}{1} P\,(1 - P)^{\varphi_{\nu m} - 1} \approx \varphi_{\nu m} P \tag{29}$$

in place of $P_{\nu m}$. Mathematically speaking, the equation $p\,(P) = \delta v/V$ now requires to be inverted, with P denoting a generalization of p in terms of δx_i (> 0). These calculations are carried out in Appendix C, where Flory's result turns out to be perturbed as follows $(d = \mathrm{L}, \mathrm{C}, \mathrm{P})$:

$$\ln \Omega_{2d} \approx \ln \Omega_{2n} + \ln \omega_{2d} \tag{30}$$

where $S_{2d} = \ln \Omega_{2d}$ is the recalculated perfect gas entropy function, $S_{2n} = \ln \Omega_{2n}$ is Flory's result and the second sum over states on the right is a perturbation of statistical nature. One therefore obtains, minus some additive constant:

$$\frac{1}{\nu} \ln \omega_{2L} = \xi_L \sum_i \alpha_i^{-1} \quad \text{(Laplace)} \tag{31}$$

$$\frac{1}{\nu} \ln \omega_{2C} = \xi_C \sum_i \alpha_i^{-2} \quad \text{(Cauchy)} \tag{32}$$

$$\frac{1}{\nu} \ln \omega_{2P} = \xi_P \sum_i \alpha_i^{-1} \quad \text{(Poisson)} \tag{33}$$

The coefficients $\xi_d \geq 0$ couple the elementary volume scale, characteristic of crosslink fluctuations, to the background elastic medium. A behavior of Cauchy's type is found as well for the Gaussian distribution, $\omega_{2n} \approx \omega_{2C}$, while Laplace's and Poisson's coupling terms turn out to coincide in the exponential limit and generally fulfill $\xi_L \leq \xi_P$ (Appendix C).

3. Notes on Strain Energy and Invariants

In subsection (2.1) it was shortly recalled that the Helmholtz free energy is the key concept to relate strain energy to the entropy function. A question thus arises of which formal representations may be induced in all generality by the statistical mechanics pictures in the former paragraphs. As a detailed analysis of constitutive laws in invariant tensor form would take us too far from the central aims of this study, we will limit ourselves to discussing the strain energy density for the present cases (U_j; $j = n, L, C, P$). We therefore suppose to deal with hyperelastic (or Green elastic) elastomers, and there exists a function $U = U(\{\alpha_k\})$ so that the stress power per unit referential volume descends from its material derivative. For simplicity, and uniformity with the previous analysis, the Cartesian notation $k = x, y, z$ is retained in what follows, though it could promptly be extended to any system of principal axes, say $k \to k' = 1, 2, 3$. Then we know that for an isotropic sample, $U = U(\mathbf{F}) \equiv U[I_i(\mathbf{C}), I_{ii}(\mathbf{C}), I_{iii}(\mathbf{C})]$, where:

$$I_i(\mathbf{C}) \;=\; \mathrm{Tr}(\mathbf{C}) \;=\; \alpha_x^2 \;+\; \alpha_y^2 \;+\; \alpha_z^2 \tag{34}$$

$$I_{ii}(\mathbf{C}) \;=\; \tfrac{1}{2}\left[\mathrm{Tr}^2(\mathbf{C}) \;-\; \mathrm{Tr}(\mathbf{C}^2)\right] \;=\; \alpha_x^2\alpha_y^2 \;+\; \alpha_y^2\alpha_z^2 \;+\; \alpha_z^2\alpha_x^2 \tag{35}$$

$$I_{iii}(\mathbf{C}) \;=\; \mathrm{Det}(\mathbf{C}) \;\equiv\; \mathrm{J}^2 \;=\; \alpha_x^2\alpha_y^2\alpha_z^2 \tag{36}$$

are the linear, quadratic and cubic principal invariants of the Cauchy-Green right tensor (Spencer, 1971), expressed on the right in terms of principal stretches. The incompressibility constraint reduces the strain energy dependence to $U = U[I_i(\mathbf{C}), I_{ii}(\mathbf{C})]$, for the Cauchy stress tensor reads:

$$\mathbf{T} \;=\; -p\mathbf{I} \;+\; 2\left(\frac{\partial U}{\partial I_i} \;+\; I_i\frac{\partial U}{\partial I_{ii}}\right)\mathbf{B} \;-\; 2\frac{\partial U}{\partial I_{ii}}\mathbf{B}^2 \tag{37}$$

where $\mathbf{I}$ and $\mathbf{B} = \mathbf{F}\mathbf{F}^T$ are respectively the identity and Cauchy-Green left (or Finger's) tensors, the latter owing the same eigenvalues and principal invariants of $\mathbf{C}$ (Amabili, 2018). Eq. (37) stems from the three-fold dependence of U upon $\mathrm{J} = \mathrm{Det}(\mathbf{F}) = 1$ and $-2J(\partial U/\partial I_{iii}) = p$. Once the energy is explicited in terms of α_k, it clearly identifies a symmetric function of principal stretches, moreover, the principal Cauchy stress components get back to Eq. (1).
In summary, mechanical models are in a way complementary to mesoscopic approaches. To capture the stress-stretch relation in homogeneous and isotropic (dry or swollen) elastomers, a free energy law can be set as a function of strain tensor invariants, and a number of advanced models with highly complicated energy behaviors were put forward with a number of phenomenological coefficients making up for the knowledge at the molecular level (Mihai and Goriely, 2017; Hossain and Steinmann, 2013). However, no one could ever rule out that different energy functions, provided with the same parameters, may predict the mechanical response equally well (Okumura, Kondo and Ohno, 2016).
With this in mind, let us consider which strain energy forms turn out to be suggested by the found entropy functions. To this end, it suffices referring to the configurational Eqs. (18-22) complemented by the perfect gas Eqs. (30-33), which bring to Eqs. (52-55) of the next subsection (4.1). Fundamental aspects of constitutive theories, mostly mathematical in nature (e.g. when quadratic form energies are positive definite in linear elasticity theory, or polyconvexity constraints apply in nonlinear regimes) won't be dealt with hereinafter, although they are reported to be often bypassed by the same scientists working in the field (Puglisi and Saccomandi, 2016). Our Gaussian response, modified by the small scale perturbation, points out the following dependence on the strain invariants:

$$\tfrac{1}{\nu}\ln\Omega_{_n} \;=\; -\,\tfrac{1}{2}I_i \;+\; \tfrac{1}{2}\ln\sqrt{I_{iii}} \;+\; \xi_n\frac{I_{ii}}{I_{iii}} \tag{38}$$

thence, the strain energy form induced by an isochoric process is generally of the Mooney & Rivlin type (Mooney, 1940):

$$U_{_n}(I_i, I_{ii}) \;=\; C_{_1}\left(I_i \;-\; I_i^*\right) \;+\; C_{_2}\left(I_{ii} \;-\; I_{ii}^*\right) \tag{39}$$

the asterisk denoting the values taken in the undeformed state, $I_i^* = I_{ii}^* = 3$, the phenomenological constants $C_{_1}$ and $C_{_2}$ being two material coefficients whose mechanical meaning is to be adjusted afterwards the best fit to experimental

data (Puglisi and Saccomandi, 2016), with C_2 taking potentially negative values as well (Mihai, Woolley and Goriely, 2019). When $\xi_n = 0$, the constitutive law becomes neo-Hookean ($C_2 = 0$) and $2C_1$ identifies the classical shear modulus (Amabili, 2018). It is interesting to note that, in the compressible case ($I_{iii} \neq 1$), the ratio I_{ii}/I_{iii} appears in Blatz & Ko model, proposed for a class of (isotropic) foam rubber materials (Blatz and Ko, 1962).
The other statistical mechanics views are somewhat more complicated, but may be expressed in terms of $I_V = \sum_i \alpha_i$ and $I_{1/V} = \sum_i 1/\alpha_i$, functions of principal stretches characterizing Varga's model (Varga, 1966; Hill and Arrigo, 1995):

$$U_V(I_i, I_{ii}, I_{iii}) = C_1(I_V - I_V^*) + C_2\sqrt{I_{iii}}\,(I_{1/V} - I_{1/V}^*) \tag{40}$$

with reference values $I_V^* = I_{1/V}^* = 3$ and, generally:

$$I_{iii}I_{1/V}^2 = I_{ii} + 2\sqrt{I_{iii}}I_V = \tfrac{1}{2}\,(I_V^2 - I_i)^2 \tag{41}$$

Accordingly, in an isochoric transformation, the strain energy density in Laplace's statistics is of Varga's type:

$$U_L(I_i, I_{ii}) = U_V(I_V, I_{1/V}) \tag{42}$$

A square root dependence on the quadratic invariant, $I_{1/V} = (I_{ii} + 2I_V)^{\frac{1}{2}}$, takes place in Carroll's model for vulcanized rubbers (Carroll, 2011). Strain functions I_V, $I_{1/V}$ are also met in Cauchy's and Poisson's statistics. The implicit relation to be regarded in the former is:

$$\prod_i (1 + \alpha_i) = \sqrt{I_{iii}}\,(I_{1/V} + 1) + I_V + 1 \tag{43}$$

so that:

$$U_C(I_i, I_{ii}) = C_1 \ln(I_V + I_{1/V} - I_C^*) + C_2(I_{ii} - I_{ii}^*) \tag{44}$$

with $I_C^* = 6$. A logarithmic behaviour is classically found in Gent models for limited chain extensibility (Gent, 1996). Poisson's statistics display instead a constitutive law like:

$$U_P(I_i, I_{ii}) = U_L(I_V, I_{1/V}) + u_P \tag{45}$$

where u_P is highly nonlinear, as it depends on the Gamma function, and is hardly expressible in terms of strain invariants straight away. For the moment, a most convenient way to focus on this behavior is to frame it between former Laplace's and a general Ogden model (see e.g. Ogden and Hill (1972)), being:

$$u_P(I_i, I_{ii}, I_{iii}) = \sum_{pqh} O_{pqh}(I_i - I_i^*)^p(I_{ii} - I_{ii}^*)^q(I_{iii} - I_{iii}^*)^h \tag{46}$$

for some tensor $\mathbf{O}$ of materials coefficients, and upon the isochoric constraint $I_{iii} = I_{iii}^* = 1$. Concluding this section, we may remark that all such constitutive relations point towards a necessary dependence on the second strain invariant I_{ii}, as it was also emphasized by other authors (Anssari-Benam, Bucchi and Saccomandi, 2021). The perturbation to the perfect gas term, likely the most affected by network details at the junction scale (i.e. chemical functionality, topology, etc.), breaks the neo-Hookean symmetry even in the (modified) Gaussian-like statistics. Except for this case, however, strain energy laws in the other incompressible rubber-like models are not separable functions of I_i and I_{ii}, and seem to display a more complex behavior. Their analysis may thereby represent an interesting issue left for future work. The matching between phenomenological coefficients and polymeric parameters will be addressed through the experimental and numerical analysis of paragraphs 5 and 6. First we need to evaluate, in the next section, the actual mechanical response in some cases of fundamental interest.

4. Mechanical Properties of Unswollen and Swollen Networks

The expressions for $\ln\Omega$ can be used to obtain the mechanical features (uniaxial) and shear stresses, σ and τ; elastic and shear moduli, E and G) in uniaxial tensile deformation (D_{U}) and pure shear deformation (D_{S}) experiments. In a swelling phenomenon, the material is characterized by an initial (ϕ_0, before swelling) and a final (ϕ, before deformation) value of polymer volume fraction, the quantity $\mathrm{Q} = \phi_0/\phi$ generalizing the former Jacobian condition, i.e. $\mathrm{J}^2 = \mathrm{Det}\ \mathbf{C} = (\mathrm{Det}\ \mathbf{F})^2 = 1$ to:

$$\prod_i \alpha_i = \mathrm{Q} \tag{47}$$

If the initial network is in dry state ($\phi_0 = 1$), the former equation identifies the (equilibrium) swelling ratio in a fully swollen permanent network ($\mathrm{Q} > 1$), where mechanical modulus and osmotic (or mixing) pressure balance each other without disrupting the essential skeletal structure (Flory and Rehner, 1943b). Otherwise, provided the polymer chains are not too stiff, nothing forbids to work as well in the shrinking or collapse domain ($\mathrm{Q} < 1$). In either case, we will consider the following deformation geometries, representative of uniaxial (tensile) deformation (D_{U}) and pure shear (D_{S}) (Arruda and Boyce, 1993; Flory, 1953):

$$\mathrm{D}_{U}(\alpha_i, \mathrm{Q}) = \{\alpha_i \mid \alpha_x \equiv \mathrm{Q}^{\frac{1}{3}}\alpha,\ \alpha_y = \alpha_z = \mathrm{Q}^{\frac{1}{3}}\alpha^{-\frac{1}{2}}\} \tag{48}$$

$$\mathrm{D}_{S}(\alpha_i, \mathrm{Q}) = \{\alpha_i \mid \mathrm{Q}^{-\frac{1}{3}}\alpha_x = \mathrm{Q}^{\frac{1}{3}}\alpha_y^{-1} \equiv \alpha,\ \alpha_z = \mathrm{Q}^{\frac{1}{3}}\} \tag{49}$$

both held at fixed temperature (T) and volume. Stretch components in the previous two definitions define the deformation gradient $\mathbf{F}$. We provide now with a separate account of such two mechanical frameworks, grouping the relevant calculations in Appendix D. It should be reminded that, although swelling can induce cavity formations inside spherical elastic matrices (Pence and Tsai, 2006), this possibility is disregarded here as we assume that (uniform) swelling establishes without application of a load. It will be supposed, in other words, that swelling precedes the occurrence of deformation implied by the external load.

4.1. Uniaxial Deformation

Consider a state of uniaxial stress (here, in the α_x direction) and the related homogeneous deformation. The stress component $\sigma \equiv \sigma_x$ produced by the elastic retraction force stems from differentiating the Helmholtz free energy, and reads (Flory, 1953):

$$\sigma = -\frac{k_B T}{V_0 \mathrm{Q}}\left(\frac{\partial \ln\Omega}{\partial\alpha}\right)_{T,V} \tag{50}$$

where the so-called engineering strain is related to the α value as $\varepsilon = \alpha - 1$, and equilibrium Young's modulus in the limit of small deformations is ($\alpha \approx 1$):

$$E \approx \sigma/\varepsilon \tag{51}$$

In Eqn. (50), k_B is still Boltzmann's constant, T the absolute temperature and V_0 the reference volume in which the crosslinking phenomenon occurred. We resume again the complete expressions of the configuration integral deduced in each case, i.e. (minus some additive entropy constant):

$$\frac{1}{\nu}\ln\Omega_L = -(\alpha_x + \alpha_y + \alpha_z) + \frac{1}{2}\ln(\alpha_x\alpha_y\alpha_z) + \xi_L\left(\alpha_x^{-1} + \alpha_y^{-1} + \alpha_z^{-1}\right) \quad \text{(Laplace)} \tag{52}$$

$$\frac{1}{\nu}\ln\Omega_C = -2\ln\left[(1+\alpha_x)(1+\alpha_y)(1+\alpha_z)\right] + \frac{1}{2}\ln(\alpha_x\alpha_y\alpha_z) + \xi_C\left(\alpha_x^{-2} + \alpha_y^{-2} + \alpha_z^{-2}\right) \quad \text{(Cauchy)} \tag{53}$$

$$\frac{1}{\nu}\ln\Omega_P \approx -l_P\left[\alpha_x + \alpha_y + \alpha_z + \frac{1}{2}\ln(\alpha_x\alpha_y\alpha_z)\right] + \sum_i \Xi_\lambda\left[\frac{\ln\lambda}{t}\ln\Gamma(\alpha_i t)\right] + \xi_P\left(\alpha_x^{-1} + \alpha_y^{-1} + \alpha_z^{-1}\right) \quad \text{(Poisson)} \tag{54}$$

where, in the last, $l_{_P} = 1 - \frac{2\ell}{\ln\lambda}$ ($\ell = 0.577$ is Euler's constant), the sum refers to an isotropic system (see Eqs. 22 - 23, Eqs. B.18 - B.19) and its contributions to the mechanical response are worked out in Appendix D. In this framework, ideal polymer networks would obey:

$$\frac{1}{\nu}\ln\Omega_{_n} \approx -\frac{1}{2}\left(\alpha_x^2+\alpha_y^2+\alpha_z^2\right) + \frac{1}{2}\ln(\alpha_x\alpha_y\alpha_z) + \xi_{_n}\left(\alpha_x^{-2}+\alpha_y^{-2}+\alpha_z^{-2}\right) \quad \text{(Gauss)} \tag{55}$$

which gets back to Flory's expression upon $P \to p$ ($\omega_{_{2n}} \to 1$) e.g. when the coupling extent 'shrinks' from an interlinking volume to a network point ($\xi_{_n} \to 0$). It is known in fact that mechanical features get normally reduced by larger fluctuations (i.e. with increasing ξ_d). Substituting Eqns. (52 - 55) into Eqn. (50) yields, upon Eqn. (48):

I. *Laplace* :

$$\sigma_{_L} = \frac{1}{3}E_{_F}\mathrm{Q}^{-\frac{2}{3}}(1-\alpha^{-\frac{3}{2}})(1-\xi_{_L}\mathrm{Q}^{-\frac{2}{3}}\alpha^{-\frac{1}{2}}) \tag{56}$$

$$E_{_L} \approx \frac{1}{3}E_{_F}\mathrm{Q}^{-\frac{2}{3}}\frac{1-\alpha^{-\frac{3}{2}}}{\alpha-1}(1-\xi_{_L}\mathrm{Q}^{-\frac{2}{3}}\alpha^{-\frac{1}{2}}) = E_{_F}\mathrm{Q}^{-\frac{2}{3}}[\frac{1}{2}(1-\xi_{_L}\mathrm{Q}^{-\frac{2}{3}}) + - \frac{5}{8}(1-\frac{7}{5}\xi_{_L}\mathrm{Q}^{-\frac{2}{3}})(\alpha-1) + \frac{35}{48}(1-\frac{59}{35}\xi_{_L}\mathrm{Q}^{-\frac{2}{3}})(\alpha-1)^2 - \ldots] \tag{57}$$

II. *Cauchy* :

$$\sigma_{_C} = \frac{2}{3}E_{_F}\mathrm{Q}^{-\frac{2}{3}}\left[\frac{1}{1+\mathrm{Q}^{\frac{1}{3}}\alpha} - \frac{1}{\alpha(\sqrt{\alpha}+\mathrm{Q}^{\frac{1}{3}})} - \xi_{_C}\mathrm{Q}^{-1}(1-\alpha^{-3})\right] \tag{58}$$

$$E_{_C} \approx \frac{2}{3}E_{_F}\left[\frac{\mathrm{Q}^{-\frac{2}{3}}}{\alpha-1}\left(\frac{1}{1+\mathrm{Q}^{\frac{1}{3}}\alpha} - \frac{1}{\alpha(\sqrt{\alpha}+\mathrm{Q}^{\frac{1}{3}})}\right) - \xi_{_C}\mathrm{Q}^{-\frac{5}{3}}\alpha^{-3}(1+\alpha+\alpha^2)\right] =$$
$$E_{_F}\mathrm{Q}^{-\frac{2}{3}}\left\{\frac{1}{(1+\mathrm{Q}^{\frac{1}{3}})^2} - 2\xi_{_C}\mathrm{Q}^{-1} - \frac{1}{4}\left[\frac{5+7\mathrm{Q}^{\frac{2}{3}}}{(1+\mathrm{Q}^{\frac{1}{3}})^3} - 16\,\xi_{_C}\mathrm{Q}^{-1}\right](\alpha-1) + + \frac{1}{24}\left[\frac{35+76\mathrm{Q}^{\frac{1}{3}}+59\mathrm{Q}^{\frac{2}{3}}}{(1+\mathrm{Q}^{\frac{1}{3}})^4} - 160\,\xi_{_C}\mathrm{Q}^{-1}\right](\alpha-1)^2 - \ldots\right\} \tag{59}$$

III. *Poisson* :

$$\sigma_{_P} \approx \frac{1}{3}E_{_F}\mathrm{Q}^{-\frac{2}{3}}(1-\alpha^{-\frac{3}{2}})(l_{_P}-\xi_{_P}\mathrm{Q}^{-\frac{2}{3}}\alpha^{-\frac{1}{2}}) \tag{60}$$

$$E_{_P} \approx \frac{1}{3}E_{_F}\mathrm{Q}^{-\frac{2}{3}}\frac{1-\alpha^{-\frac{3}{2}}}{\alpha-1}(l_{_P}-\xi_{_P}\mathrm{Q}^{-\frac{2}{3}}\alpha^{-\frac{1}{2}}) = E_{_F}\mathrm{Q}^{-\frac{2}{3}}[\frac{1}{2}(l_{_P}-\xi_{_P}\mathrm{Q}^{-\frac{2}{3}}) + - \frac{5}{8}(l_{_P}-\frac{7}{5}\xi_{_P}\mathrm{Q}^{-\frac{2}{3}})(\alpha-1) + \frac{35}{48}(l_{_P}-\frac{59}{35}\xi_{_P}\mathrm{Q}^{-\frac{2}{3}})(\alpha-1)^2 - \ldots] \tag{61}$$

the Gaussian results becoming:

$$\alpha\,\frac{\Delta\sigma_{_{FQ}}}{\sigma_{_F}} = \frac{\Delta E_{_{FQ}}}{E_{_F}} = -2\xi_{_n}\mathrm{Q}^{-\frac{4}{3}} \tag{62}$$

with $\Delta\sigma_{FQ} = \sigma_{nQ} - \sigma_{FQ}$ and $\Delta E_{FQ} = E_{nQ} - E_{FQ}$ now denoting the variations between modified and pure Gaussian values. Note that Flory's relations are promptly recovered, i.e.:

$$\frac{\sigma_{FQ}}{\sigma_F} = \frac{E_{FQ}}{E_F} = \mathrm{Q}^{-\frac{1}{3}} \tag{63}$$

where, as usual:

$$\sigma_F = \tfrac{1}{3}\varepsilon E_F(1+\alpha^{-1}+\alpha^{-2}) , \tag{64}$$

and:

$$E_F = 3\rho k_B T \tag{65}$$

is Flory's elastic modulus for an unswollen network as a function of the number density of polymer strands, $\rho = \nu/V_0$. As expected, the original expressions for a Gaussian system are regained upon $\xi_n \to 0$ in Eqn. (62).

4.2. Pure Shear

Analogously to the former subsection, Helmholtz free energy (per unit volume) allows to connect the configuration integral to the shearing stress as well (Flory, 1953):

$$\tau = -\frac{k_B T}{V_0 \mathrm{Q}}\left(\frac{\partial \ln \Omega}{\partial \gamma}\right)_{T,V} \tag{66}$$

and hence to the equilibrium shear modulus in infinitesimal deformations, still related to the slope of stress-strain curve near the zero-strain point ($\alpha \approx 1$):

$$G \approx \tau/\gamma \tag{67}$$

As the shear strain can be taken on to be $\gamma = \alpha - 1/\alpha$ (Flory, 1953), the expressions generated by Eqs. (52 - 54) under Eq. (49) now are:

I. *Laplace* :

$$\tau_L = G_F \mathrm{Q}^{-\frac{2}{3}} \frac{\alpha^2-1}{\alpha^2+1}(1-\xi_L \mathrm{Q}^{-\frac{2}{3}}) \tag{68}$$

$$G_L \approx G_F \mathrm{Q}^{-\frac{2}{3}} \frac{\alpha}{\alpha^2+1}(1-\xi_L \mathrm{Q}^{-\frac{2}{3}}) = G_F \mathrm{Q}^{-\frac{2}{3}}(1-\xi_L \mathrm{Q}^{-\frac{2}{3}})\left[\tfrac{1}{2} - \tfrac{1}{4}(\alpha-1)^2 + \ldots\right] \tag{69}$$

II. *Cauchy*:

$$\tau_C = 2G_F \mathrm{Q}^{-\frac{2}{3}}\left[\frac{\alpha^2}{1+\alpha^2}\left(\frac{1}{\mathrm{Q}^{\frac{1}{3}}\alpha+1} - \frac{1}{\alpha(\mathrm{Q}^{\frac{1}{3}}+\alpha)}\right) - \xi_C \mathrm{Q}^{-1}\gamma(\alpha)\right] \tag{70}$$

$$G_C \approx 2G_F \mathrm{Q}^{-\frac{2}{3}}\left[\frac{\alpha^2}{(\alpha^2+1)(\mathrm{Q}^{\frac{1}{3}}+\alpha)(\mathrm{Q}^{\frac{1}{3}}\alpha+1)} - \xi_C \mathrm{Q}^{-1}\right] = G_F \mathrm{Q}^{-\frac{2}{3}}\left[\frac{1}{(1+\mathrm{Q}^{\frac{1}{3}})^2} - 2\xi_C \mathrm{Q}^{-1} - \tfrac{1}{2}\frac{1+4\mathrm{Q}^{\frac{1}{3}}+\mathrm{Q}^{\frac{2}{3}}}{(1+\mathrm{Q}^{\frac{1}{3}})^4}(\alpha-1)^2 + \ldots\right] \tag{71}$$

III. *Poisson* :

$$\tau_P = G_F \mathrm{Q}^{-\frac{2}{3}} \frac{\alpha^2-1}{\alpha^2+1}(l_P - \xi_P \mathrm{Q}^{-\frac{2}{3}}) \tag{72}$$

$$G_{_P} \approx\ G_{_F}\mathrm{Q}^{-\frac{2}{3}}\frac{\alpha}{\alpha^2+1}(l_{_P}-\xi_{_P}\mathrm{Q}^{-\frac{2}{3}})\ =\ G_{_F}\mathrm{Q}^{-\frac{2}{3}}(l_{_P}-\xi_{_P}\mathrm{Q}^{-\frac{2}{3}})\left[\tfrac{1}{2}-\tfrac{1}{4}\,(\alpha-1)^2+\ ...\ \right] \quad (73)$$

where, with similar notations to Eqn. (62), the relationships:

$$\frac{\Delta\tau_{_F}}{\tau_{_{FQ}}}\ =\ \frac{\Delta G_{_F}}{G_{_{FQ}}}\ =\ -\,2\xi_{_n}\mathrm{Q}^{-\frac{4}{3}} \quad (74)$$

$$\frac{\tau_{_{FQ}}}{\tau_{_F}}\ =\ \frac{G_{_{FQ}}}{G_{_F}}\ =\ \mathrm{Q}^{-\frac{1}{3}} \quad (75)$$

still represent modified Flory's predictions for a swollen Gaussian network, with:

$$\tau_{_F}=\ G_{_F}\gamma \quad (76)$$

$$G_{_F}=\ \tfrac{1}{3}E_{_F}=\ \rho k_{_B}T \quad (77)$$

Again, unperturbed results can be retrieved upon $\xi_n \to 0$ in Eqs. (74).

4.3. Theoretical Remarks

Figure (1) reports a sketchy relationship among Gaussian, Cauchy's and exponential-like distributions in one dimension, the last category including Laplace's and Poisson's. Three main regions for the polymer end-to-end distance can be crudely identified, delimited for simplicity by the probability axis and two vertical dashed lines. In comparison with the Gaussian, polymer ends in Cauchy's and exponential chains tend to be more spaced out both at small and intermediate length scales. At small scales, exponential distributions stand for the most repulsive of the three classes, Cauchy's taking their place in the halfway region. Quite the contrary, the likelihood to find two Gaussian ends at larger distances is the least, whereas Cauchy's chains display the largest attraction. The specific way by which such mutual statistical weights (or chain interactions) may emerge falls outside the aim of this study. What matters here is to point out that, whenever the polymer network could be driven outside the Gaussian state, it would still be possible to resort to a consistent and fairly applicable framework. Different mechanical responses than Flory's then can be sensed and analyzed at the experimental level.

Accordingly, expressing the previous results in units of $\sigma_{_F}$ or $E_{_F}$ quantifies at once the discrepancies one would get from adopting the other statistics in place of the Gaussian's. Laplace's and Poisson's predictions differ as expected by the coefficient $l_{_P}=1-2\ell/\ln\lambda>1$, determined in isotropic materials ($\lambda_i\equiv\lambda$) at second order in the exponential regime (see Appendices B and D). Since $\lambda\approx(1.25\cdot10^{-1}\div5)\cdot10^{-2}$ implies $l_{_P}\approx(1.15\div1.4)$, Poisson-like moduli would be approximately $\approx(20\div40)$ % larger than the corresponding exponential values.

The terms ξ_d are proportional to a mean coupling parameter of order h, defined in Appendix C as $\xi_h\approx\frac{1}{3}\sum_i(\delta x_i/x_{_{0i}})^h$ ($h=2$ for Gauss's and Cauchy's statistics, $h=1$ for Laplace's and Poisson's). An evaluation of it may be given through relative fluctuation weights (or volume fractions), $\xi_h\approx(\delta V/V_{_0})^{h/3}$, i.e. the portion of space swept out on the average by crosslinked units owing to energy sources and constraints. Scattering experiments showed that cross-links undergo simultaneous translational and orientational diffusion, not dissimilar in magnitude from the chain gyration radius, and connecting its ends on the ns time scale (D. Stein, A. Hoffman, Frank and D. Fayer, 1992). By neglecting elastic constraints produced by network connections, the variance of junction fluctuations can be derived from the stiffness tensor (Erman and Flory, 1982b). However, Eq. (74) may be used to prompt a relationship with the cycle rank in the phantom model (Rubinstein and Colby, 2003), $G/G_{_F}=1-2/f$, adopted in the following as to set a Gaussian reference state to which normalizing any other phenomenological coefficient. In a perfect network, with $f/2$ strands per crosslink, it evaluates the difference between the numbers of elastically effective strands and crosslinks, and is believed to be suitable especially for diluted systems e.g. gels). In our case, confronting Eq. (74) with it identifies:

$$\xi_{_n}=\ \frac{\mathrm{Q}^{\frac{4}{3}}}{f} \quad (78)$$

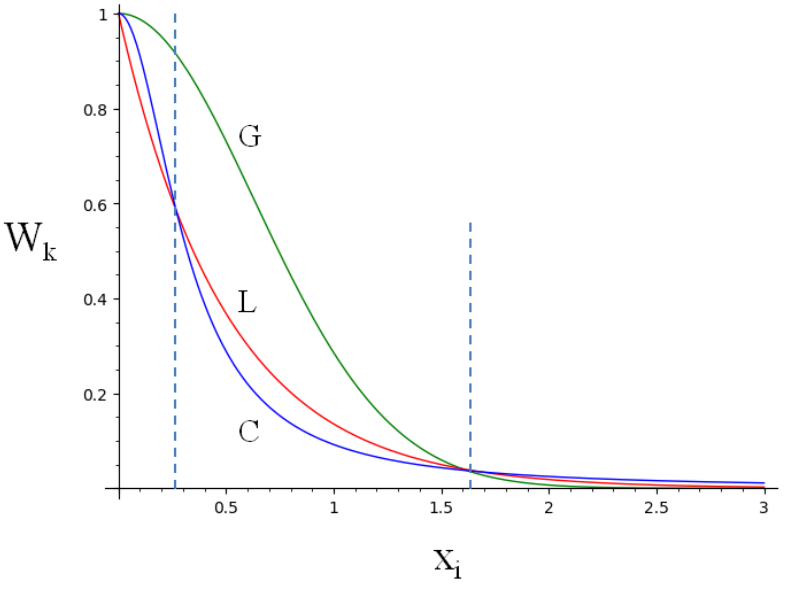

Figure 1: Gaussian (G, green), Cauchy's (C, blue), Laplace's (L, red) end-to-end distribution functions with zero average and normalized in one dimension to $W_k(x_k = 0) = 1$. As being a statistics of exponential type, Poisson's should be regarded in this scheme as to fall into the L category.

and, correspondingly:

$$\xi_L = \sqrt{3/(2\pi f)}\, Q^{\frac{2}{3}} \quad \text{(Laplace)} \tag{79}$$

$$\xi_C = \xi_n \quad \text{(Cauchy)} \tag{80}$$

$$\xi_P = l_P \xi_L \quad \text{(Poisson)} \tag{81}$$

In imperfect networks, cycle rank should take the influence of dangling chains and loops into account. Network defects, however, are not going to be examined here, nor chain dimension ratios or front factors. Conceptually, they don't lead to significant changes of classical theories (e.g. Flory's (Eichinger, 2015)) and would not alter the conclusions we will come to later.

5. Materials and Methods

The three hydrogels studied, based on alginate, agar and scleroglucan, find a wide spreading in biomedical field for their peculiar properties such as biocompatibility and giving rise to strong and weak hydrogels in mild conditions (Matricardi et al., 2016). Alginate is a collective term to describe a family of polysaccharides isolated from brown seaweeds and bacteria (Donati and Paoletti, 2009). Chemically, alginates are linear copolymers of $1 \rightarrow 4$ linked β-d-mannuronic acid (MM) and its C-5 epimer, α-l-guluronic acid (GG), arranged in a blockwise pattern, with homopolymeric regions of MM- and GG residues, indicated as MM-blocks and GG-blocks, respectively, and interspersed with regions of alternating structure (MG blocks). The ability to form stable physical hydrogels upon treatment with divalent ions, such as calcium's (Draget, Smidsrand Skjåk-Bræk, 2005), have resulted in alginates being widely used in industrial and

biomedical applications. For example, they have been used for encapsulation of insulin-producing Langerhans islets for treatment of type I diabetes (de Vos, Bučko, Gemeiner, Navrátil, Švitel, Faas, Strand, Skjak-Braek, Morch, Vikartovská, Lacík, Kolláriková, Orive, Poncelet, Pedraz and Ansorge-Schumacher, 2009) and as drug delivery systems (Matricardi, Meo, Coviello, Hennink and Alhaique, 2013). The higher the GG content, the stiffer and more fragile is the gel they form in water in presence of divalent cations. Alginate used in this paper (molecular weight $\approx 10^6$ Da), a kind gift from FMC Biopolymer Ltd, UK, was characterized by a high GG content ($\approx$ 70 % GG and 30 % MM). In order to prepare the hydrogel, a proper amount of alginate powder was slowly added to stirred distilled water contained in a beaker at room temperature up to forming a homogeneous solution (alginate mass fraction 0.02; % mass fraction = 2%). A proper amount of alginate solution then was poured into a bottom flat beaker to get a film of thickness $\approx$ 1 mm. Subsequently, a $CaCl_2$ water solution (Ca^{2+} concentration = 5 g/l) was rapidly sprayed on the gel surface to promote alginate crosslinking (volume of sprayed crosslinking solution was approximately equal to the gel volume). After 5 min of contact, the solution was removed and the crosslinked film was immediately and gently cleaned by laboratory paper. Upon formation, the gel was cut into 35 mm diameter disks (thickness $\approx$ 1 mm) by means of a stainless-steel punch with the same diameter of the rheometer sensor. In case of LF-NMR tests, the gel was cut into $\approx$ 8 mm diameter disks ($\approx$ 1 mm thick) and put inside the LF-NMR glass tube.

Agar is a gel forming polysaccharide with a main chain consisting of alternating 1, 3-linked β-D-galactopyranose and 1, 4-linked 3, 6 anhydro-α-L-galactopyranose units (Arnott, Fulmer, Scott, Dea, Moorhouse and Rees, 1974). It is composed by agarose and agaropectin (Labropoulos, Niesz, Danforth and Kevrekidis, 2002). Agarose is a neutral polysaccharide and represents the fraction with gelling capacity while agaropectin contains the charged polysaccharide components. Agarose and agaropectin contents depend on the seaweed source which agar is extracted from and affects physicochemical, mechanical and rheological properties of the gels (Labropoulos et al., 2002). It has been suggested that the agarose network arises from double helix formation and subsequent aggregation into bundles, called suprahelices (Labropoulos et al., 2002; Djabourov, Clark, Rowlands and Ross-Murphy, 1989). However, according to molecular modeling studies (Kouwijzer and Pérez, 1998), agarose appears to be capable of creating both single- and double- helical structures, which are left-handed and antiparallel-packed. As expected for a gel-forming polysaccharide, all of the proposed crystal structures show enough available space ($30 - 45$ %) for water molecules. The agar considered in this paper (molecular weight $\approx 1.2 \cdot 10^5$ Da), supplied by Biokar (Diagnostics, France), was of alimentary grade, i.e. essentially composed by agarose. Agar gel was realized by dissolving 1 g of polymer into 99 g of distilled water at 90° C, so that the polymer mass fraction in final gels was 0.01 (% mass fraction = 1%). The solution was homogenized and poured into proper vessels to allow gelation due to cooling at room temperature. For rheological characterization, the vessel used was a cylinder $\approx$ 2 mm thick with a diameter of $\approx$ 50 mm. Again, the formed gel was cut into 35 mm diameter disks by means of a stainless-steel punch with the same diameter of the rheometer sensor. About NMR tests, the solution was poured directly inside the LF-NMR glass tube.

Scleroglucan is a nonionic polysaccharide secreted exocellularly by fungi of genus Sclerotium. Its primary structure consists of a linear backbone of (1,3)-β-linked d-glucopyranosyl residues bearing a single (1,6)-β-linked d-glucopyranosyl unit every three sugar residues of the main chain (Rinaudo and Vincendon, 1982). Both in aqueous solution and the solid state, scleroglucan adopts a highly ordered, rigid, triple helical tertiary structure (triplex), which consists of three individual strands composed by six residues in the backbone per turn. The three triplex strands are held together by inter-strand H-bonds at the center of the triplex. The $(1 \rightarrow 6)$-linked β-d-glucopyranosyl side groups protrude from outside the triplex, preventing intermolecular aggregation and polymer precipitation (Bluhm, Deslandes, Marchessault, Pérez and Rinaudo, 1982; Fariña, Sineriz, Molina and Perotti, 2001; Palleschi, Bocchinfuso, Coviello and Alhaique, 2005a). Triplex conformation is destabilized only in dimethyl sulfoxide or strong alkaline conditions, and characterized by a high rigidity, responsible for the peculiar properties exhibited by aqueous scleroglucan solutions in a wide pH range and even at relatively high temperatures. As triplex clustering increases, the formation of three-dimensional hydrogel networks takes place (this happens, typically, for a polymer mass fraction (Grassi, Lapasin and Pricl, 1996) $\geq$ 0.0025). Owing to its rheological properties, scleroglucan is used as thickener and suspending agent in several industrial sectors (Lapasin and Pricl, 1995). In addition, as it is biocompatible, biodegradable and bio-adhesive, it is widely used in cosmetics and pharmaceutics fields, its main application being the release of bioactive molecules (Coviello, Grassi, Lapasin, Marino and Alhaique, 2003; Grassi, Lapasin, Coviello, Matricardi, Di Meo and Alhaique, 2009; Matricardi, Onorati, Coviello and Alhaique, 2006; Viñarta, François, Daraio, Figueroa and Fariña, 2007). Scleroglucan used in this study (Actigum CS11) was provided by Cargill (Minneapolis, MN, USA) and characterized by an average molecular weight of $1.2 \cdot 10^6$ Da. The hydrogel (polymer mass fraction 0.02; 2%) was prepared by gradually adding the polymer powder to distilled water under mechanical stirring at room temperature. Just after preparation, the system

was kept in fridge at temperature of 8°C for 24 h in order to promote the gel formation. The weak gel nature allowed to easily put it in the rheometer sensor and LF-NMR glass tube by the aid of a spatula.

5.1. Low-Field NMR

The end-to-end distribution, of the polymeric network pervading the studied hydrogels, was determined by means of Low-Field NMR, looking at the magnetic relaxation of hydrogen units of water molecules trapped in the network. Information on the network architecture (mesh size distribution) thus was gained indirectly by recording the effect of polymeric chains (the solid hydrogel component) on magnetically relaxing water hydrogens. Because of the very fast process, magnetic relaxation of hydrogen units of polymer chains did not affect our measurements.
Water protons relaxation time T_2 was measured by means of a Bruker Minispec mq20 (0.47 T, 20 MHz, Germany) at 25°C resorting to the CPMG (Carr-Purcell-Meiboom-Gill) (Meiboom and Gill, 1958) sequence {90°[-τ-180°-τ(echo)]$_n$-T_R} with a 8.36 μs wide 90° pulse, $\tau = 250$ μs, $T_R = 10$ s (sequence repetition rate), n being the number of detected experimental intensities. The criterion to deem the relaxation process over and choose the value of n was to wait for the FID (Free Induction Decay) intensity reaching about 2% of its initial value. Each relaxation experiment, composed by n points, was repeated 36 times (four scans each of 9 repetitions performed). The continuous T_2 distribution was determined by fitting the experimental FID ($I_s(t)$) by the following equation (Whittall and MacKay, 1989):

$$\mathrm{I(t)} \;=\; \int_{\mathrm{T_{2min}}}^{\mathrm{T_{2max}}} a(\mathrm{T_2}) \exp\left(-\frac{\mathrm{t}}{\mathrm{T_2}}\right) \mathrm{dT_2} \tag{82}$$

where T_{2max} and T_{2min} indicate, respectively, the smallest and largest values of the continuous T_2 distribution, $a(T_2)$ is the unknown amplitude of the spectral component at relaxation time T_2, while exp(-t/T_2) represents the decay term. In order to fit Eq. (82) to the experimental FID ($I_s(t)$) and get the continuous T_2 distribution (A_i vs T_{2i}), the following discretization scheme was adopted (Whittall and MacKay, 1989):

$$\mathrm{I(t)} \;\approx\; \sum_{\mathrm{i=1}}^{\mathrm{N}} a_{\mathrm{i}} \exp\left(-\mathrm{t}/\mathrm{T_2^i}\right)\left(\mathrm{T_2^{i+1}} - \mathrm{T_2^i}\right) \;=\; \sum_{\mathrm{i=1}}^{\mathrm{N}} \mathrm{A_i} \exp\left(-\mathrm{t}/\mathrm{T_2^i}\right) \tag{83}$$

where the range of the T_2 distribution (T_{2min} - T_{2max}) was logarithmically subdivided into $N = 200$ parts (larger N values were proven to be unnecessary).
Because of some noise disturbing the measure of I_s, the fitting procedure must not minimize the χ^2 statistics, but a smoothed definition (Whittall and MacKay, 1989) of it (χ_s^2):

$$\chi_{\mathrm{s}}^2 = \sum_{\mathrm{i=1}}^{\mathrm{N}} \left(\frac{\mathrm{I_s\left(t_i\right) - I\left(t_i\right)}}{s_{\mathrm{i}}}\right)^2 + \mu \sum_{\mathrm{i=1}}^{\mathrm{N-2}} \left|\mathrm{A_{i+2} - 2A_{i+1} + A_i}\right|^2 \tag{84}$$

where σ_i is the i^{th} datum standard deviation, and μ is weighting the smoothing term as proposed by Provencher (Provencher, 1982). Although different criteria can be followed for determining μ, we adopted the strategy proposed by Wang (Wang and Ni, 2003), according to which the correct value is pointed out just below the heel (slope variation) of the plot $\ln\chi_s$ vs $\ln\mu$.
The continuous T_2 profile can be transformed into hydrogel mesh size distribution by resorting to the Fiber-Cell (Chui, Phillips and McCarthy, 1995) and Scherer theories (Scherer, 1994). To this purpose, it was recently demonstrated that, for a hydrogel polymer volume fraction $\phi < 0.61$, the average mesh size ζ deriving from the Scherer theory can be properly approximated by (Abrami, Chiarappa, Farra, Grassi, Marizza and Grassi, 2018):

$$\zeta \;=\; \mathrm{R_f}\sqrt{\frac{\mathrm{C_1}}{\mathrm{C_0}}\left(\frac{1 - 0.58\phi}{\phi}\right)} \tag{85}$$

where R_f is the radius of the polymeric chain (imagined to be a long cylinder), while C_1 and C_0 are two constants depending on the mesh architecture which for a cubic mesh are equal, respectively, to 1 and 3π. In light of Eq. (85), the Fiber-Cell theory (Chui et al., 1995) leads to the following relation between ζ and the average value of the reciprocal

of relaxation time $(1/T_2)_m$:

$$\left(\frac{1}{\mathrm{T_2}}\right)_{\mathrm{m}} = \frac{1}{\mathrm{T_{2H2O}}} + \frac{2\mathcal{M}}{\zeta\sqrt{\frac{\mathrm{C_0}}{\mathrm{C_1}}\left(\frac{1-0.58\phi}{\phi}\right)}} \tag{86}$$

$$\left(\frac{1}{\mathrm{T_2}}\right)_{\mathrm{m}} = \sum_{\mathrm{i=1}}^{\mathrm{N}} \frac{\mathrm{A_i}}{\mathrm{T_{2i}}} \tag{87}$$

in which T_{2H2O} is the bulk proton relaxation time (i.e. the water proton relaxation time in the absence of polymer, the so-called free water relaxation time ≈ 3000 ms at 25°C and 0.47 T) (Coviello, Matricardi, Alhaique, Farra, Tesei, Fiorentino, Asaro, Milcovich and Grassi, 2013) and $\mathcal{M}$ (length/time) is the 'relaxivity', a parameter accounting for the surface effect of polymer chains on water proton relaxation. In fact, $\mathcal{M}$ is the ratio between thickness and relaxation time of the bound water layer adhering to the solid surface (Chui et al., 1995). While Eq. (86) holds, on average, for all the polymeric network meshes, similar expressions can be written for meshes of different dimensions (ζ_i) by assuming $\mathcal{M}$ to be independent of the mesh size (Chui et al., 1995):

$$\frac{1}{\mathrm{T_{2i}}} = \frac{1}{\mathrm{T_{2H2O}}} + \frac{2\mathcal{M}}{\zeta_{\mathrm{i}}\sqrt{\frac{\mathrm{C_0}}{\mathrm{C_1}}\left(\frac{1-0.58\phi}{\phi}\right)}} \tag{88}$$

T_{2i} being the relaxation time of water protons trapped in polymer meshes of size ζ_i. The bi-univocal correspondence between T_{2i} and ζ_i only holds in the fast-diffusion regime, i.e when mobility of water molecules, expressed by their self-diffusion coefficient (Holz, Heil and Sacco, 2000) D ($2.09 \cdot 10^{-9}$ m^2/s at 25°C), is large as compared to the rate of magnetization loss, identifiable with $R_c\ \mathcal{M}$ (i.e. $R_c\mathcal{M}$/D ≪1). In fact in the slow diffusion regime, relaxation of all water protons contained in the volume of a mesh of size ζ_i is not described by only one T_{2i} but a multiplicity of T_{2i}. R_c, indicating the radial distance from polymer chain axis at which the effect of polymeric chains on water proton relaxation gets negligible, can be expressed by (Chui et al., 1995):

$$\mathrm{R_c} = \frac{\mathrm{R_f}}{\sqrt{\phi}} \tag{89}$$

The combination of Eqs.(86) and (88) allows to conclude that the ratio between ζ_i and its maximum value, ζ_{max}, is influenced exclusively by the relaxation times T_{2i} and T_{2max} (apart from the free water relaxation time T_{2H2O}):

$$\zeta_{\mathrm{i}}^{+} = \frac{\zeta_{\mathrm{i}}}{\zeta_{\mathrm{max}}} = \frac{\left(\frac{1}{\mathrm{T_{2max}}} - \frac{1}{\mathrm{T_{2H2O}}}\right)}{\left(\frac{1}{\mathrm{T_{2i}}} - \frac{1}{\mathrm{T_{2H2O}}}\right)} \tag{90}$$

Thus, as Eq. (90) yields a way to convert relaxation times into mesh size, it does not require the knowledge of the two parameters R_f and ϕ, whose determination is not always straightforward. Accordingly, the probability $P_i(\zeta_i{}^+)$ of finding a mesh of size $\zeta_i{}^+$ inside the polymer network writes:

$$\mathrm{A_i}\left(\zeta_{\mathrm{i}}^{+}\right) = \mathrm{A_i}\left(\mathrm{T_{2i}}\right), \quad \mathrm{P_i}\left(\zeta_{\mathrm{i}}^{+}\right) = \frac{\mathrm{A_i}\left(\zeta_{\mathrm{i}}^{+}\right)}{\sum_{\mathrm{i=1}}^{\mathrm{N}} \mathrm{A_i}\left(\zeta_{\mathrm{i}}^{+}\right)} \tag{91}$$

where coefficients $A_i(T_{2i})$ are known from Eq. (83) fitting the experimental relaxation data.

5.2. End-to-end Size Distribution

Starting from the distribution of cubic meshes in Eqs. (90) - (91), it is possible determining the end-to-end size distribution, i.e. the distribution of vectors moduli representing the length (end-to-end distance) of polymer segments extending from a fixed crosslink to the next one along a given primary polymer molecule. To this aim, though other

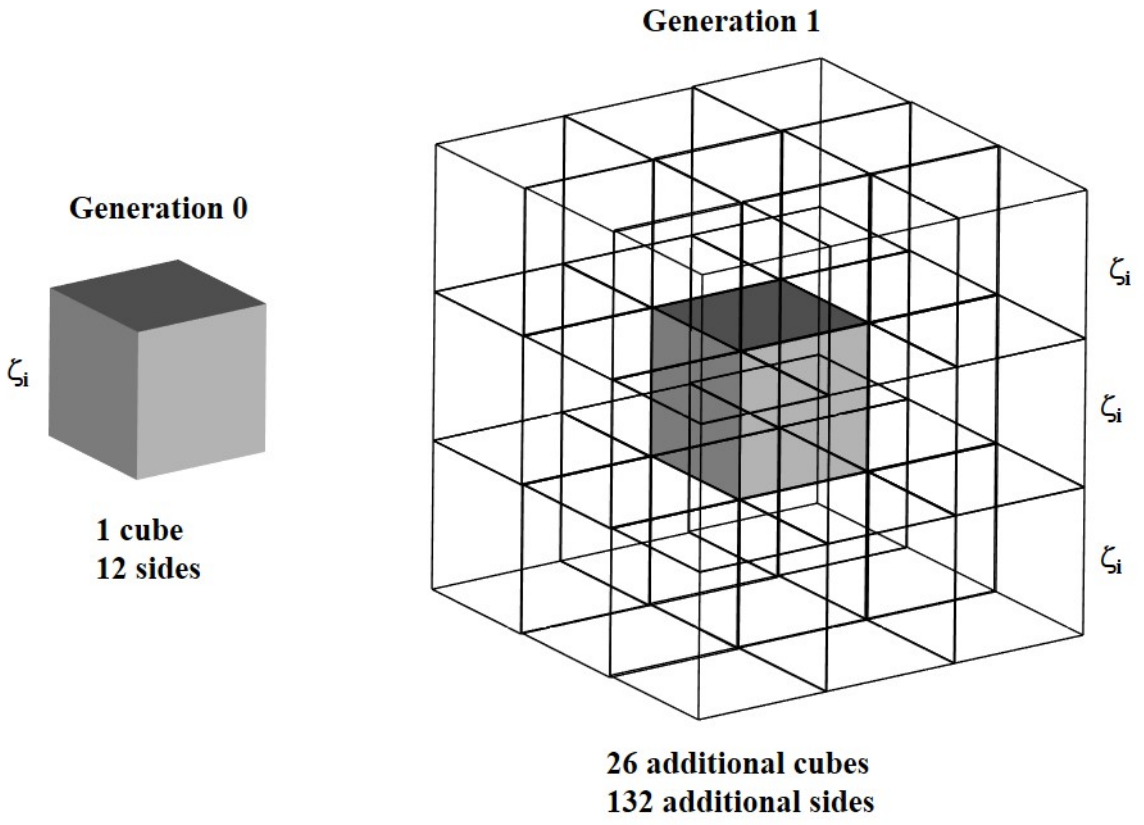

Figure 2: The polymeric network is generated by covering the 'seed cube' (generation 0, size ζ_i) by other identical cubes (generation 1). This covering process, repeated up to generation n_i, gives rise to a polymeric network with cubic mesh size ζ_i.

structures may be certainly regarded, let's assume in accord with Eq. (85) that polymer meshes are cubical and the entire network can be generated equivalently by "covering" the "seed cubic mesh" of size ζ_i (generation 0; see Fig. 2) by other cubic meshes of size ζ_i (generation 1). Whilst generation 1 requires considering further 26 cubes (3^3 cubes minus the seed cube), the number of new cube sides are not $26 \cdot 12$, as further cubes share several sides, and it is easy to verify the additional sides are only 132. In order to further expand the network, we can repeat such an operation by covering the cubic structure of size $3\zeta_i$ by other 26 cubes of size $3\zeta_i$ (generation 2) and so on, up to generation n_i. Accordingly, the number of additional cubes and sides at generation 2, 3, .. n_i are those indicated in Table (1).

Generation	**Additional cubes**	**Additional sides**
0	1	12
1	26	132
2	$26 \cdot 3^3$	$132 \cdot 3$
3	$26 \cdot 3^6$	$132 \cdot 3^2$
n_i	$26 \cdot 3^{3(n_i-1)}$	$132 \cdot 3^{(n_i-1)}$

Table 1. Geometric characteristics of a network after n_i generations.

Considering that a real network is not composed by meshes of identical size ζ_i but, more realistically, it comprises different meshes with sizes spanning from ζ_1 to ζ_N ($\zeta_1 < \zeta_2 < .. \ \zeta_i \ .. < \zeta_N$), we assume it to come from summing the meshes of all dimensions. On the basis of the discussion reported in Appendix E, it can be demonstrated that the fraction of meshes (F_{Mi}) and sides (F_{Si}) of size ζ_i are related to the probability $P_i(\zeta_i^+)$ (Eq. 91) of finding a mesh of

size $\zeta_i{}^+$ in the polymeric network by:

$$F_{Mi}\% = \frac{P_i}{\sum_{i=1}^{N} P_i} \tag{92}$$

$$F_{Si} = \frac{\sqrt[3]{P_i}}{\sum_{i=1}^{N} \sqrt[3]{P_i}} \tag{93}$$

In conclusion, Eq. (93) allows to convert the mesh size distribution, as determined by LF-NMR characterization in Eq. (90), into the end-to-end size distribution, as required by the rubber elasticity theory.

5.3. Rheology

Rheological measurements were performed at 25°C by a stress controlled rotational rheometer (Haake Mars Rheometer, 379-0200 Thermo Electron GmbH, Karlsruhe, Germany) equipped with parallel plate geometry (PP35, diameter = 35 mm, with serrated surfaces to avoid slippage at the wall) and a gap of $\approx (1 \div 2)$ mm. The measuring device was kept inside a glass bell at saturated humidity conditions to avoid evaporation effects. In order to assess the shear modulus (G) dependence on shearing deformation (γ), stress sweep tests, led at 1 Hz, were performed on each hydrogel. This dependence is given by Eq. (67), where both shear deformation and stress (τ) were experimentally determined.

6. Results and Discussion

6.1. Small deformations

It seems reasonable starting the theoretical comparison among the original Flory theory and the results derived in this paper by focusing the three end-to-end distance distributions (i.e. Poisson, Laplace, Cauchy) in the limit of small shear deformations. Fig. (3) shows the trend of the ratio between the new shear moduli (G, from Poisson's, Laplace's, Cauchy's statistics) and Flory's (G_F, Eq. 77) versus the swelling (Q > 1) or shrinking (Q < 1) ratio. This comparison was performed by assuming vanishing shear deformations, a high functionality value ($f = 45$) and the same crosslink density in crosslinking conditions (Q = 1; reference state). It can be seen that the ratio G/G_F (see Eqs. 69, 71, 73) decreases with increasing Q whatever the considered distribution is. Moreover, with Laplace's and Cauchy's statistics, one always has $G/G_F < 1$.

On the contrary, when Q ≤ 0.2, Poisson's distribution yields a ratio > 1. It is important to underline that a similar behavior is found for smaller f, even though the Cauchy distribution provides with physically consistent results in the whole Q domain when crosslink fluctuations are rather small (large f values). In addition, owing to the small deformation hypotheses ($E = 3G$, see also Eq. 77), all the above considerations hold with uniaxial deformations as well. Finally, it is interesting recalling that the results shown in Fig. (3) can be seen from a different viewpoint that is closer to the polymeric network architecture. In light of the equivalent network theory (Schurz, 1991), it is possible indeed transforming the results in Fig. (3) in terms of the average network mesh size:

$$\zeta = \sqrt[3]{\frac{6}{\pi N_A \rho_x}} \tag{94}$$

N_A being Avogadro's number and ρ_x being the molar crosslink density (crosslink moles per unit volume). Eq. (94) implies:

$$\frac{\zeta_k}{\zeta_F} = \sqrt[3]{\frac{\rho_{xF}}{\rho_{xk}}} \tag{95}$$

where ρ_{xF} and ρ_{xk} indicate, respectively, the crosslink density in original Flory's work and those in Laplace's, Cauchy's and Poisson's distributions, while ζ_F and ζ_k similarly denote the average mesh size descending from Flory's and the new statistical distributions. As the ratio ρ_{xF}/ρ_{xk} does not depend on Q, ζ_k/ζ_F is always equal to 0.765, 0.590 and 0.835, respectively (taking on $l_p = 1.3$, see Theoretical Remarks). Adopting non-Gaussian statistics therefore reduces the average value of mesh size, at least in the cases hereby regarded.

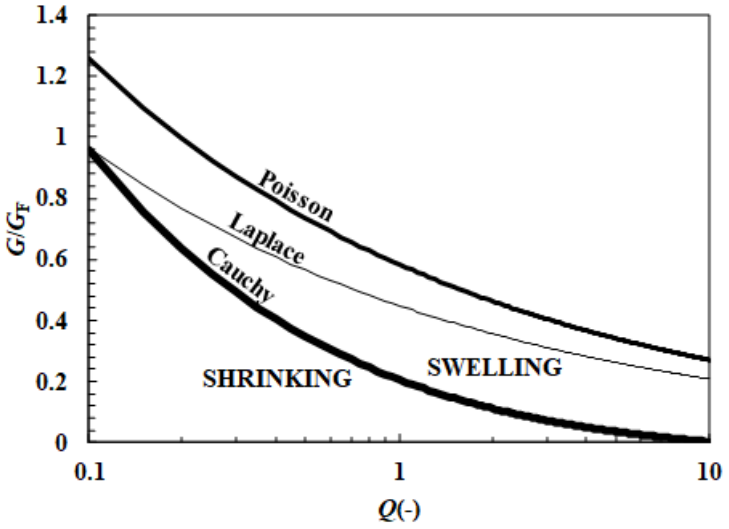

Figure 3: Theoretical comparison amongst the shear modulus descending from the Gaussian theory ($G_{_F}$) and those (G) in Eq. (69) (Laplace), Eq. (71) (Cauchy), Eq. (73) (Poisson) in the limit $\gamma \to 0$ ($\alpha \to 1$). It is performed in both shrinking/swelling domains (Q = 1 stands for the crosslink density in the reference state) with a large functionality value ($f = 45$).

6.2. Large deformations

With large deformations, one of the most interesting aspects is the dependencies of Young's and shear moduli on uniaxial (ε) and pure shear (γ) deformations, respectively. To this purpose, it is worth remembering that in the original Flory theory $G_{_F}$ does not depend on γ while the elastic modulus decreases with ε. Combining Eq. (64) and Eq. (65) and remembering that $\rho_x = \rho/N_A$, one explicitly has:

$$\mathrm{E}^*_{\mathrm{F}} \;=\; RT\rho_{\mathrm{xF}}\mathrm{Q}^{-\frac{1}{3}}\left[1+\frac{1}{\varepsilon+1}+\frac{1}{(\varepsilon+1)^2}\right] \tag{96}$$

It is interesting to study the trend of $E/E^*_{_F}$ and $G/G_{_F}$ versus deformation for the three distributions here considered plus the one coming from the modified Flory theory, implemented by the factor ζ_n (see Eq. 55) upon Q = 1 and f = 10. Fig. (4) makes clear that whatever ε, Young's modulus in Flory's theory is always larger than any other (including the modified Flory's) and the ratio $E/E^*_{_F}$ does not sensibly depend on ϵ for all distributions except from Laplace's, as it increases with increasing ϵ. For pure shear deformations (Fig. 5), the shear modulus from Flory's theory is always larger than in other distributions, the ratio $G/G_{_F}$ being almost constant.
A most important aspect suggested by these non-Gaussian distributions is that shear modulus is affected by γ. This points out a clear generalization of Flory's theory, setting $E^*_{_F}$ to depend on ε and $G_{_F}$ to be γ-independent. Also in these simulations, large junction fluctuations ($f < 10$) lead Cauchy's distribution to return unrealistic results.

6.3. Determination of end-to-end distributions

To derive the end-to-end distribution requires Eq. (83) to be applied to experimental relaxation data (I_s(t)), here of agar, alginate and scleroglucan hydrogels as depicted, respectively, in Figs. (6), (7) and (8). This fitting reveals the relaxation time distribution (A_{2i}, T_{2i}) is characterized by only one peak in agar (Fig. 6) and scleroglucan (Fig. 8) hydrogels, while two main peaks are visible for alginate (Fig. 6). This is simply due to the fact that, after crosslinking, the alginate gel tends to contract by expelling water (syneresis) that accumulates among the hydrogel disks filling the LF-NMR glass tube. The position of the second peak shown in Fig. (7) is very close in fact to the free water relaxation time at 25°C (3000 ms, 0.47 T) (Coviello et al., 2013). Only the first peak is indicative of water molecules trapped inside the polymer network, this being the reason why the second one will no longer be considered. On the contrary, the single peak characterizing agar (Fig. 6) and scleroglucan (Fig. 8) time distributions are representative of trapped

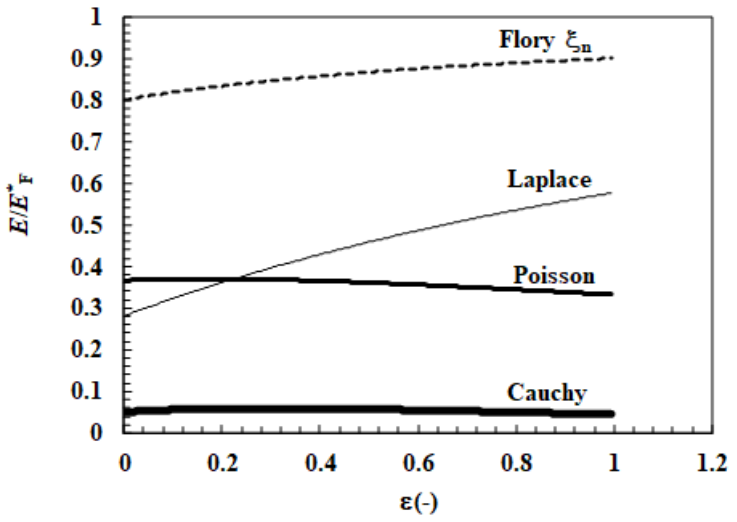

Figure 4: Dependence on the uniaxial deformation (ε) of the ratio E/E^*_F, between the Young modulus (E) implied by the three distributions (Laplace, Eq. 57; Cauchy, Eq. 59; Poisson, Eq. 61) plus the ones from Flory's theory implemented by the ξ_n factor (Eq. 55) and Flory's E^*_F. Simulations were performed with swelling ratio Q = 1 and network connectivity f = 10.

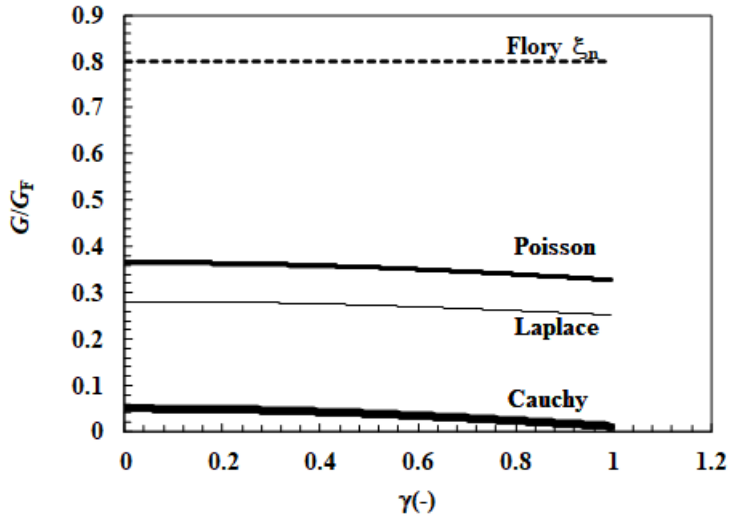

Figure 5: Dependence on the shearing deformation (γ) of the ratio G/G_F, between the shear modulus (G) in Eq. (69) (Laplace), Eq. (71) (Cauchy), Eq. (73) (Poisson) and Flory's Eq. (77) (G_F). Simulations were performed with a swelling ratio Q = 1 and network functionality f = 10.

water molecules, as they are very far from the free water relaxation time. Eqs. (90) - (91) allow us to convert the relaxation time profile (A_{2i}, T_{2i}) into the mesh size (F_{Mi}, Eq. (92)) and the end-to-end (F_{Si}, Eq. (93)) distributions for the agar, alginate and scleroglucan hydrogels (depicted respectively in Figs. 9, 10, 11). F_{Mi} % and F_{Si} % represent the percentage probability of finding a mesh or an end-to-end length in the network that equals ζ_i, according to Eq. (92) and Eq. (93). The direct correspondence between relaxation time T_{2i} and mesh size ζ_i is guaranteed by the fast diffusion conditions occurring in our hydrogels. In fact, as the water self-diffusion coefficient at 25°C is (Holz et al., 2000) $2.09 \cdot 10^{-9}$ m^2/s, R_f typically spans from (Amsden, 1998; Palleschi, Bocchinfuso, Coviello and Alhaique, 2005b) 0.5 to 2.2 nm and ϕ is equal to $6.6 \cdot 10^{-3}$, $5.7 \cdot 10^{-3}$ and $12.6 \cdot 10^{-3}$ respectively in agar 1% (density = 1520

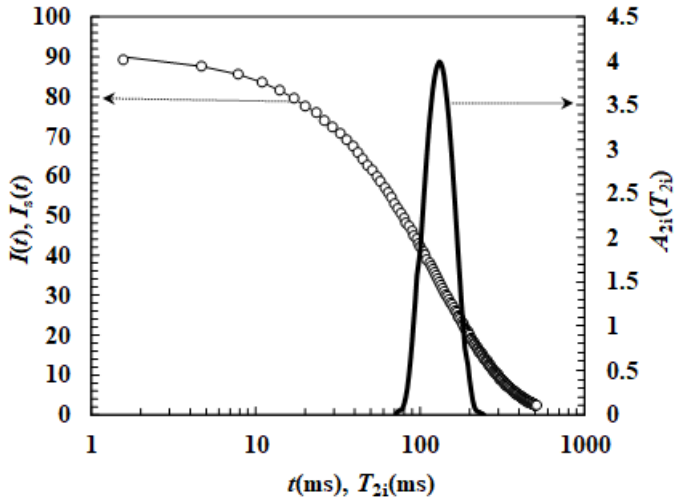

Figure 6: Best fitting Eq. (83) ($I(t)$, thin solid line: left vertical axis) to experimental relaxation data ($I_s(t)$, open circles) of agar hydrogel (smoothing factor $\mu = 150$). Best fit is represented by A_i vs T_{2i} relaxation time distribution (thick solid line; right vertical axis).

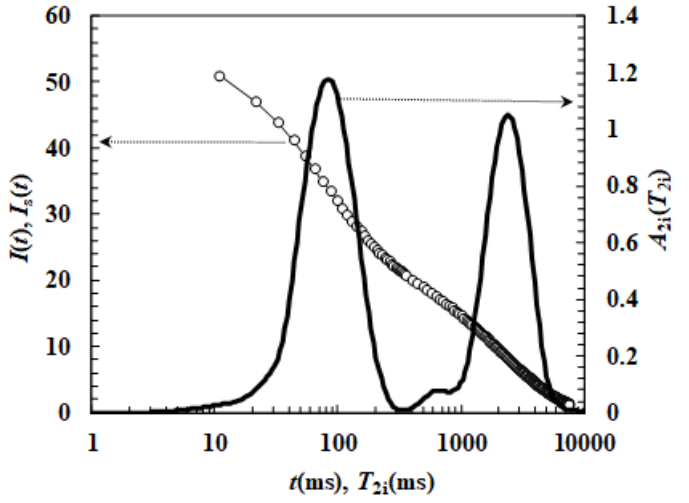

Figure 7: Best fitting Eq. (83) ($I(t)$) to experimental relaxation data ($I_s(t)$) for alginate hydrogel ($\mu = 160$). Symbols and notations as in Fig. (6).

kg/m^3) (De$'$ Nobili, Rojas, Abrami, Lapasin and Grassi, 2015), alginate 1% (density = 1770 kg/m^3) (Pasut, Toffanin, Voinovich, Pedersini, Murano and Grassi, 2008) and scleroglucan 2% (density = 1600 kg/m^3) (Coviello et al., 2013) hydrogels, then the dimensionless number $R_c\mathcal{M}/D$ is always $\ll 1$ ($\sim 10^{-5}$ - 10^{-6}). Interestingly, from the Kolmogorov-Smirnov test (Kolmogorov, 1933; Smirnov, 1948) and whatever the gel regarded, $F_{Si}\%$ turns out not to be normally distributed, thus the study of other statistical distributions would be anyway in order. We thus fitted the Gauss, Laplace, Poisson and Cauchy laws with the pseudo-experimental $F_{Si}\%$ profiles for the three systems, as Figs. (12), (13) and (14) show:

$$\mathrm{F_F}\% \;=\; 100\left(\frac{\beta}{\sqrt{\pi}}\right)^3 \mathrm{e}^{-\beta^2\left(\zeta_\mathrm{i}^+-\mu_\mathrm{a}\right)^2}\Delta\zeta_\mathrm{i}^+ \tag{97}$$

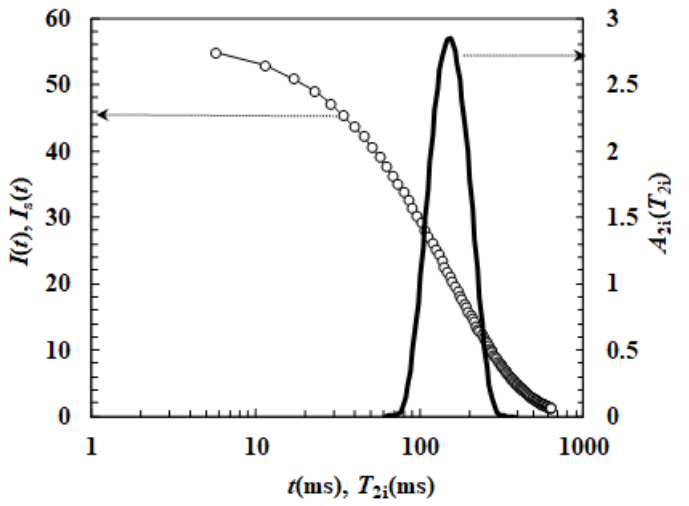

Figure 8: Best fitting Eq. (83) ($I(t)$) to experimental relaxation data ($I_s(t)$) for scleroglucan hydrogel ($\mu = 150$). Symbols and notations as in Fig. (6).

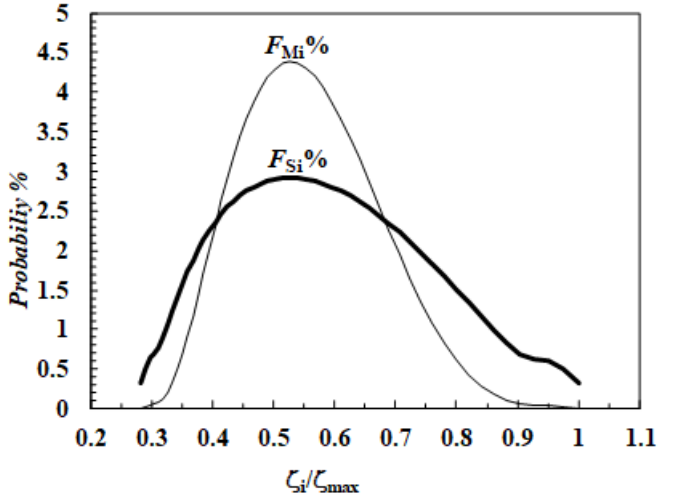

Figure 9: % mesh size ($F_{Mi}\%$) and end-to-end ($F_{Si\%}$) distributions for agar hydrogel. ζ_i and ζ_{max} are, respectively, the i^{th} mesh size and the maximum mesh size values.

$$\mathrm{F_L}\% = 50\mathrm{L}\, \mathrm{e}^{-\mathrm{L}|\zeta_\mathrm{i}^+ - \mu_\mathrm{a}|} \Delta\zeta_\mathrm{i}^+ \tag{98}$$

$$\mathrm{F_P}\% = 100\, \frac{\lambda^{\zeta_\mathrm{i}^+} \ln\left(\frac{1}{\lambda}\right)\, \mathrm{e}^{0.577\zeta_\mathrm{i}^+}}{\prod_{\mathrm{k}=1}^{\infty} \mathrm{e}^{\zeta_\mathrm{i}^+/\mathrm{k}} / \left(1+\zeta_\mathrm{i}^+/\mathrm{k}\right)} \Delta\zeta_\mathrm{i}^+ \qquad 0 < \lambda \ll 1 \tag{99}$$

$$\mathrm{F_C}\% = \frac{\mathrm{C}/\pi}{\left(\zeta_\mathrm{i}^+ - \mu_\mathrm{a}\right)^2 + \mathrm{C}^2} \Delta\zeta_\mathrm{i}^+ \tag{100}$$

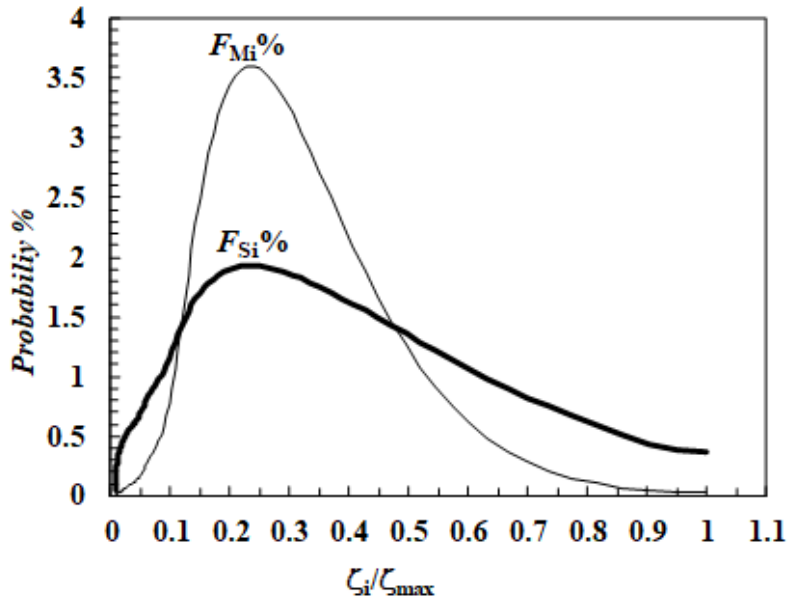

Figure 10: % mesh size (F_{Mi}%) and end-to-end ($F_{Si\%}$) distributions for alginate hydrogel. Symbols and notations as in Fig. (9).

where $\zeta_i^+ = \zeta_i/\zeta_{max}$ is a dimensionless end-to-end length, F_F%, F_L%, F_P%, F_C% are the % probability of finding in the network an end-to-end distance within ζ_i^+ and $\zeta_i^+ + \Delta\zeta_i^+$, according to the Gauss (F), Laplace (L), Poisson (P) and Cauchy (C) statistics, μ_a denotes the average value while, as in our former notations, β, L, λ and C are parameters which stem from adopting Gauss, Laplace, Poisson and Cauchy laws. Fig. (12) and Table (2) immediately reveal that, while Poisson's distribution cannot statistically fit F_{Si}% data (F test failed), every other was able to (F test was positive).

Agar 1% hydrogel (Fig. 12)				
GAUSS	$\beta = 2.34 \pm 0.03$	$\mu_a = 0.37 \pm 0.01$	$F(1,51,0.95) < 181$	AIC = - 86
LAPLACE	$L = 5.80 \pm 0.31$	$\mu_a = 0.50 \pm 0.01$	$F(1,51,0.95) < 113$	AIC = - 72
POISSON	-		-	-
CAUCHY	$C = 0.13 \pm 0.01$	$\mu_a = 0.51 \pm 0.01$	$F(1,51,0.95) < 53$	AIC = - 48
Alginate 1% hydrogel (Fig. 13)				
GAUSS	$\beta = 2.50 \pm 0.02$	$\mu_a = -0.037 \pm 0.006$	$F(1,104,0.95) < 933$	AIC = - 341
LAPLACE	$L = 5.15 \pm 0.17$	$\mu_a = 0.154 \pm 0.005$	$F(1,104,0.95) < 433$	AIC = - 270
POISSON	$\lambda = 0.015 \pm 0.001$		$F(1,105,0.95) < 2881$	AIC = - 526
CAUCHY	$C = 0.143 \pm 0.007$	$\mu_a = 0.167 \pm 0.007$	$F(1,104,0.95) < 268$	AIC = - 233
Scleroglucan 2% hydrogel (Fig. 14)				
GAUSS	$\beta = 2.45 \pm 0.03$	$\mu_a = 0.20 \pm 0.01$	$F(1,51,0.95) < 260$	AIC = - 70
LAPLACE	$L = 6.36 \pm 0.33$	$\mu_a = 0.34 \pm 0.01$	$F(1,51,0.95) < 1995$	AIC = - 62
POISSON	-		-	-
CAUCHY	$C = 0.118 \pm 0.009$	$\mu_a = 0.35 \pm 0.01$	$F(1,51, 0.95) < 107$	AIC = - 38

Table 2. Parameters for all distributions fitting the F_{Si}% data shown in Figs. (12), (13) and (14). AIC is Akaike's number (Burnham and Anderson, 2004).

In order to statistically point out the best model, Akaike's criterion (Burnham and Anderson, 2004) was adopted,

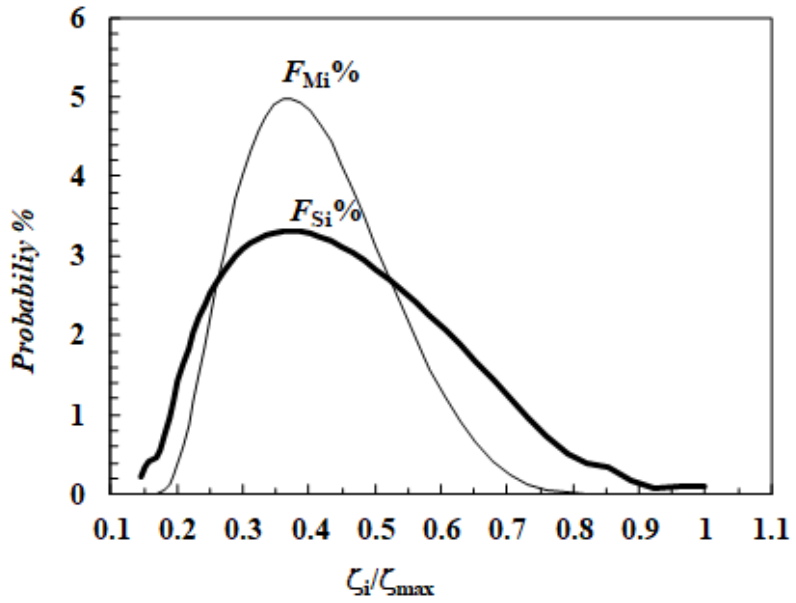

Figure 11: % mesh size (F_{Mi}%) and end-to-end ($F_{Si\%}$) distributions for scleroglucan hydrogel. Symbols and notations as in Fig. (9).

i.e. the model to be preferred will be characterized by the smallest Akaike number (*AIC*):

$$\mathrm{AIC} = \mathrm{N}\ln\left(\frac{\chi^2}{\mathrm{N}}\right) + 2\,\frac{(\mathrm{N_F}+1)\,(\mathrm{N}-\mathrm{N_F})}{\mathrm{N}-\mathrm{N_F}-2} \tag{101}$$

where N and N_F are respectively the numbers of experimental data and fitting parameters, χ^2 being the sum of squared differences between experimental data and best fit. This criterion would suggest the Gaussian's as the best distribution among those adopted (Table 2). For the alginate hydrogel (Fig. 13), all of the adopted distributions can better fit the F_{Si}% data but, on the basis of Akaike's criterion, the best model turns out to be Poissonian. This may also be expected from a visual inspection of Fig. (13) (dashed line). Finally, from Fig. (14) and Table (2), Poisson's statistics turns out to be unsuitable for scleroglucan data (F-test failed), whereas amongst the others Akaike's test would select the Gaussian law. However, as for the agar gel, none of the above distributions may be regarded as fully satisfactory (see Fig. 14).

6.4. Determination of the average mesh size

Once the best end-to end distribution is identified for each hydrogel, we can proceed with the analysis of their rheological behaviors via a proper expression for $G = G(\gamma)$. In particular, for agar and scleroglucan hydrogels, we have found that the best distribution among those here regarded is Gaussian while, for the alginate, is Poissonian. In the first two cases, however, the Gaussian statistics is not very accurate and in fact G does not behave as a constant in an ample γ domain but starts to non-linearly decrease (Fig. 15) at rather low deformation values (scleroglucan 2%, $\alpha_c \approx 1.03$; agar 1%, $\alpha_c \approx 1.001$), where network damaging is unlikely (here ν = constant). A lower crosslink density relates in turn with an increase of the average mesh size, as dictated by Eq. (77) and Eq. (94) (Q = 1):

$$\zeta = \sqrt[3]{\frac{6\mathrm{R}T}{\pi \mathrm{N}_A G}} \tag{102}$$

where R is the universal gas constant and T (= 298.15 K) is absolute temperature. Assuming for G in the last equation the average value of the linear part of $G = G(\gamma)$, as shown by Fig. (15), ($\gamma_{max} = 4.1 \cdot 10^{-3}$ for agar, $\gamma_{max} = 6.2 \cdot 10^{-2}$

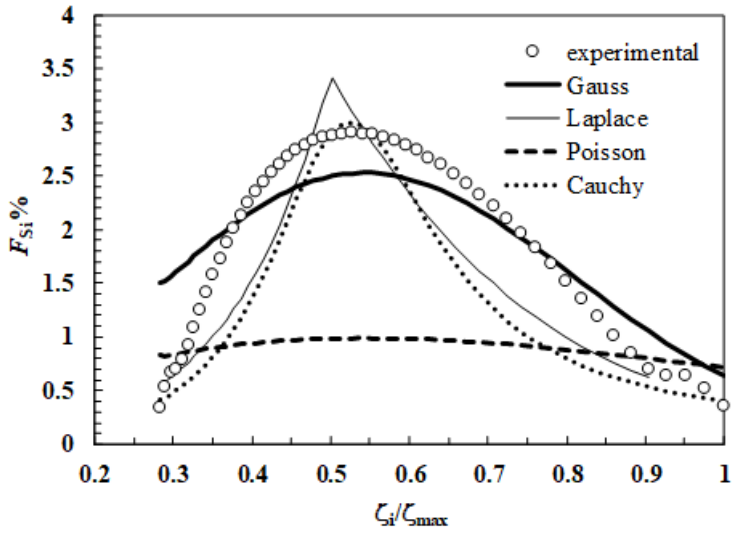

Figure 12: Best fitting the Gauss, Laplace, Poisson and Cauchy distributions (continuous, dashed and dotted lines) to the pseudo-experimental F_{Si}% profile (open circles) for the agar hydrogel (ζ_i and ζ_{max} are, respectively, the i^{th} mesh size and maximum mesh size values).

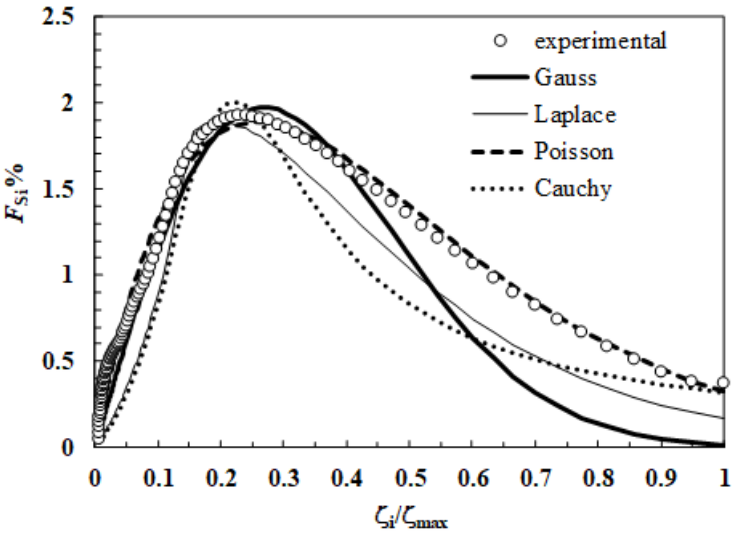

Figure 13: Best fitting the Gauss, Laplace, Poisson and Cauchy distributions to the pseudo-experimental F_{Si}% profile for the alginate hydrogel. Symbols and notations as in Fig. (12).

for scleroglucan), we get:

$$\rho_x^{agar} = 1.16 \text{ mol/m}^3 , \quad \zeta_{agar} = 14 \text{ nm} \tag{103}$$

$$\rho_x^{scl.} = 6 \cdot 10^{-2} \text{ mol/m}^3 , \quad \zeta_{scl.} = 38 \text{ nm} \tag{104}$$

In the alginate case, the $G\,(\gamma)$ expression that descends from Poisson's statistics (Eq. 73) reads:

$$\mathrm{G} = \mathrm{RT}\rho_{\mathrm{x}}(l_{_P} - \xi_{_P})\frac{\alpha}{1+\alpha^2} , \quad \alpha = \tfrac{1}{2}(\gamma+\sqrt{\gamma^2+4}) \tag{105}$$

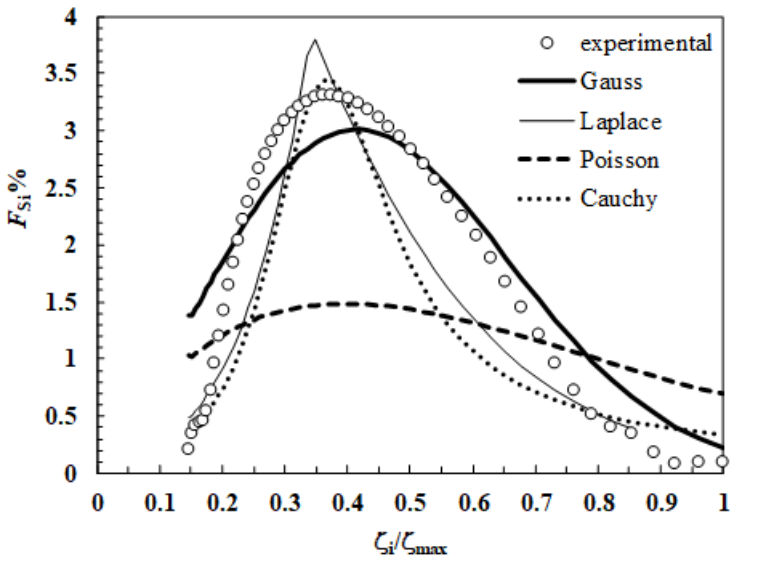

Figure 14: Best fitting the Gauss, Laplace, Poisson and Cauchy distributions to the pseudo-experimental F_{Si}% profile for the scleroglucan hydrogel. Symbols and notations as in Fig. (12).

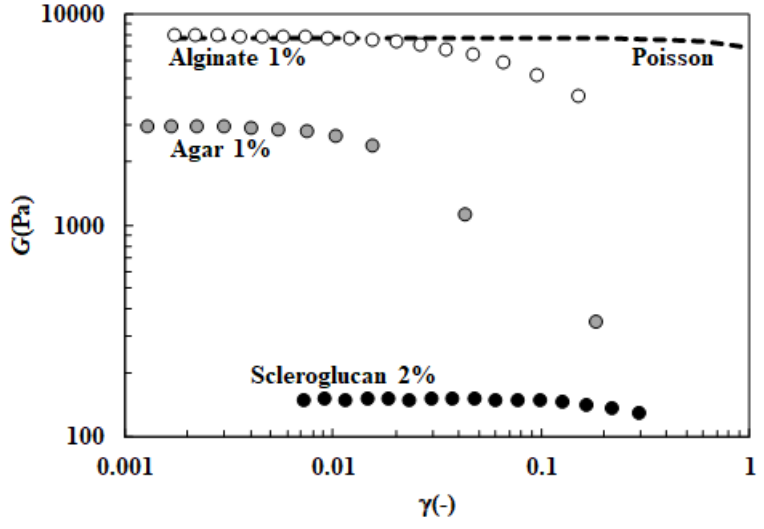

Figure 15: Dependence of shear modulus G on shearing deformation γ for the three hydrogels here considered (symbols). Dashed line denotes the $G = G(\gamma)$ trend produced by the Poisson distribution.

with ξ_P still given by Eq. (81), and:

$$l_P = 1 - 2\,\frac{0.577}{\ln\lambda} \tag{106}$$

By setting $\lambda = 0.015$ (see Table 2) and a wide range of network functionalities, $f = (4 - 1000)$, Eq. (105) was used to fit the dataset in Fig. (15) and deduce the fitting parameter ρ_x . Eq. (105) works out well for $\alpha \leq \alpha_c$ (≈ 1.01; alginate 1%), likely ascribing the recorded non-linearity of $G = G(\gamma)$ to Poisson's law corrections at larger deformations. This can be proved by limiting Eq. (105) to best fit the linear part of the experimental trend of G (dashed line in Fig. 15). The onset of nonlinear behavior foreseen by Eq. (105) occurs in fact at larger deformations, $\alpha \geq \alpha_c$. For f still varying

in the same interval, ρ_x ranges between 15.8 and 5.1 mol/m^3 and the average mesh size (ζ_{algin}) between 5.8 and 8.5 nm, i.e. a quite moderate effect.

7. Conclusions

We studied the influence of explicitly non-Gaussian statistics on elastic properties (Young and shear moduli) of hydrogels, accounting as well for the influence of possible swelling/shrinking processes after crosslinking. An account of such effects in both swollen and unswollen states required a reformulation of the statistical mechanics problem of rubber elasticity, either discussing the configuration integral or the so-called perfect gas term in formally different statistical contexts from the Gaussian's (Laplace', Poisson's, Cauchy's). In the end, the inferred new families of statistical and mechanical laws are reasonably simple for a model comparison, with strain energy densities of Mooney & Rivlin (modified Gaussian statistics) Varga (Laplace's) and Varga & Ogden (Poisson's) types. Cauchy's statistics, on the contrary, seems to put forward a new constitutive law.

Quite predictably, in all the non-Gaussian statistics here adopted, not only Young's but also the shear modulus turns out to depend on deformation, contrarily to the original Gaussian (Flory) model, where shear modulus is insensitive to it. Furthermore, for small deformations and swelling ratios $Q \geq 1$, the assumption of non-Gaussian distributions at a constant crosslink density (ρ_{x0}, crosslink reference state) yields smaller values of Young's and shear moduli than the original Flory's predictions. Only when $Q < 1$ the Poisson distribution can imply larger moduli. At a fixed Young's or shear modulus, these findings bring to larger estimates of the crosslink density and smaller average values of the network mesh size. In case of large deformations with ρ_{x0} and f held constant, such quantities result again smaller than Flory's values at whatever deformation.

To define a strategy to thoroughly check the statistical mechanics results and identify the most realistic end-to-end length distribution in the hydrogel network, a theoretical-experimental inquiry based on LF-NMR was developed. For every hydrogel hereby studied (agar 1 %; alginate 1 %; scleroglucan 2 %), statistics should be never regarded as Gaussian (Kolmogorov-Smirnov test). This is interesting as, while it could be generally expected from polymer theory, the Gaussian model still identifies the best distribution function in agar and scleroglucan gels. Quite surprisingly, Poisson's gives instead the best conformational statistics for the alginate hydrogel, especially in the low deformation regime. The possibility to deduce the most probable distribution in light of new statistical mechanics models guides the rheology interpretation by choosing the appropriate model for the mechanical moduli. Here, an onset of non-linear response develops at rather low deformation values, where network breaking remains unlikely (alginate 1%, $\alpha_c \approx 1.01$; scleroglucan 2%, $\alpha_c \approx 1.03$; agar 1%, $\alpha_c \approx 1.001$). Let the number of crossinked strands to vary with the deformation, one should better understand to which extent such experimental deviations may be ascribed to conformational statistics corrections or network damaging. This is an interesting issue left for future work. Alongside, our approach is promising to get the most probable mesh size, that is, the starting point to build up a continuous mesh size distribution of a polymer network. As a final remark, considering the number of increasingly complex polymer systems in the most varied fields of natural and engineering sciences, we hope this study will suggest the rationale and stimulate the search for new hypothesis in the field.

Acknowledgement

Bruce Eichinger (Washington University) is kindly acknowledged for sending remarks on his PRE paper.

References

Abrami, M., Chiarappa, G., Farra, R., Grassi, G., Marizza, P., Grassi, M., 2018. Use of low field nmr for the characterization of gels and biological tissues. ADMET DMPK 6, 34–46. doi:10.5599/admet.6.1.430.

Aldous, D., 1989. Exponential Combinatorial Extrema. Springer New York, New York, NY. pp. 131–148. doi:10.1007/978-1-4757-6283-9_7.

Amabili, M., 2018. Nonlinear Mechanics of Shells and Plates in Composite, Soft and Biological Materials. Cambridge University Press. URL: https://books.google.it/books?id=h5VuDwAAQBAJ.

Amsden, B., 1998. Solute diffusion within hydrogels. mechanisms and models. Macromolecules 31, 8382–8395. URL: https://doi.org/10.1021/ma980765f, doi:10.1021/ma980765f, arXiv:https://doi.org/10.1021/ma980765f.

Anssari-Benam, A., Bucchi, A., Saccomandi, G., 2021. On the central role of the invariant i_2 in nonlinear elasticity. Int. J. Eng. Sci. 163, 103486. URL: https://www.sciencedirect.com/science/article/pii/S0020722521000331, doi:10.1016/j.ijengsci.2021.103486.

Arnott, S., Fulmer, A., Scott, W., Dea, I., Moorhouse, R., Rees, D., 1974. The agarose double helix and its function in agarose gel structure. J. Mol. Biol. 90, 269 – 284. URL: http://www.sciencedirect.com/science/article/pii/0022283674903726, doi:https://doi.org/10.1016/0022-2836(74)90372-6.

Arruda, E.M., Boyce, M.C., 1993. A three-dimensional constitutive model for the large stretch behavior of rubber elastic materials. J. Mech. Phys. Solids 41, 389–412. URL: https://www.sciencedirect.com/science/article/pii/0022509693900136, doi:10.1016/0022-5096(93)90013-6.

Baek, S., Srinivasa, A., 2004. Diffusion of a fluid through an elastic solid undergoing large deformation. Int. J. Non-Lin. Mech. 39, 201 – 218. doi:https://doi.org/10.1016/S0020-7462(02)00153-1.

Baker, M., Ericksen, J., 1954. Inequalities restricting the form of the stress-deformation relations for isotropic elastic solids and reiner-rivlin fluids. J. Wash. Acad. Sci. 44, 33–35. URL: https://www.jstor.org/stable/24533303.

Ball, R.C., Edwards, S.F., 1980. Elasticity and stability of a dense gel. Macromolecules 13, 748–761. doi:10.1021/ma60075a049.

Basu, A., Wen, Q., Mao, X., Lubensky, T.C., Janmey, P.A., Yodh, A.G., 2011. Nonaffine displacements in flexible polymer networks. Macromolecules 44, 1671–1679. doi:10.1021/ma1026803.

Beatty, M., 2003. An Average-Stretch Full-Network Model for Rubber Elasticity. volume 70. pp. 65–86. doi:10.1007/1-4020-2308-1_7.

Beatty, M.F., 1987. Topics in Finite Elasticity: Hyperelasticity of Rubber, Elastomers, and Biological Tissues—With Examples. Appl. Mech. Rev. 40, 1699–1734. URL: https://doi.org/10.1115/1.3149545, doi:10.1115/1.3149545, arXiv:https://asmedigitalcollection.asme.org/appliedmechanicsreviews/article-pdf/40/12/1699/5435382/1699_1.pdf.

Bechir, H., Chevalier, L., Idjeri, M., 2010. A three-dimensional network model for rubber elasticity: The effect of local entanglements constraints. Int. J. Eng. Sci. 48, 265–274. URL: https://www.sciencedirect.com/science/article/pii/S0020722509001566, doi:10.1016/j.ijengsci.2009.10.004.

Bird, R., Armstrong, R., Hassager, O., 1990. Dynamics of Polymeric Liquids, Volume 1: Fluid mechanics, 2nd Edition. Wiley, New York.

Blatz, P.J., Ko, W.L., 1962. Application of finite elastic theory to the deformation of rubbery materials. Trans. Soc. Rheol. 6, 223–252. URL: https://doi.org/10.1122/1.548937, doi:10.1122/1.548937, arXiv:https://doi.org/10.1122/1.548937.

Bluhm, T.L., Deslandes, Y., Marchessault, R.H., Pérez, S., Rinaudo, M., 1982. Solid-state and solution conformation of scleroglucan. Carbohydr. Res. 100, 117 – 130. URL: http://www.sciencedirect.com/science/article/pii/S0008621500810307, doi:https://doi.org/10.1016/S0008-6215(00)81030-7.

Burak Erman, M.J.E., 1989. Rubber-like elasticity. Annu. Rev. Phys. Chem. 40, 351–374. doi:10.1146/annurev.pc.40.100189.002031.

Burnham, K.P., Anderson, D.R., 2004. Multimodel inference: Understanding aic and bic in model selection. Sociol. Methods Res. 33, 261–304. URL: https://doi.org/10.1177/0049124104268644, doi:10.1177/0049124104268644, arXiv:https://doi.org/10.1177/0049124104268644.

Candau, S., Bastide, J., Delsanti, M., 1982. Structural, elastic, and dynamic properties of swollen polymer networks. volume 44. pp. 27–71. doi:10.1007/3-540-11471-8_2.

Carroll, M., 2011. A strain energy function for vulcanized rubbers. J. Elast. 103, 173–187. doi:10.1007/s10659-010-9279-0.

Chan, A.W., Neufeld, R.J., 2009. Modeling the controllable ph-responsive swelling and pore size of networked alginate based biomaterials. Biomaterials 30, 6119 – 6129. URL: http://www.sciencedirect.com/science/article/pii/S0142961209007467, doi:https://doi.org/10.1016/j.biomaterials.2009.07.034.

Chui, M.M., Phillips, R.J., McCarthy, M.J., 1995. Measurement of the porous microstructure of hydrogels by nuclear magnetic resonance. J. Colloid Interface Sci. 174, 336 – 344. URL: http://www.sciencedirect.com/science/article/pii/S0021979785713999, doi:https://doi.org/10.1006/jcis.1995.1399.

Coviello, T., Grassi, M., Lapasin, R., Marino, A., Alhaique, F., 2003. Scleroglucan/borax: characterization of a novel hydrogel system suitable for drug delivery. Biomaterials 24, 2789 – 2798. URL: http://www.sciencedirect.com/science/article/pii/S0142961203000875, doi:https://doi.org/10.1016/S0142-9612(03)00087-5.

Coviello, T., Grassi, M., Rambone, G., Alhaique, F., 2001. A crosslinked system from scleroglucan derivative: preparation and characterization. Biomaterials 22, 1899–1909. URL: https://www.sciencedirect.com/science/article/pii/S0142961200003744, doi:10.1016/S0142-9612(00)00374-4.

Coviello, T., Matricardi, P., Alhaique, F., Farra, R., Tesei, G., Fiorentino, S., Asaro, F., Milcovich, G., Grassi, M., 2013. Guar gum/borax hydrogel: Rheological, low field nmr and release characterizations. Express Polym. Lett. 7, 733–746. doi:10.3144/expresspolymlett.2013.71.

Curro, J.G., Mark, J.E., 1984. A non-gaussian theory of rubberlike elasticity based on rotational isomeric state simulations of network chain configurations. ii. bimodal poly(dimethylsiloxane) networks. J. Chem. Phys. 80, 4521–4525. doi:10.1063/1.447237.

D. Stein, A., A. Hoffman, D., Frank, C., D. Fayer, M., 1992. Reorientational motion of a cross-link junction in a poly(dimethylsiloxane) network measured by time-resolved fluorescence depolarization. J. Chem. Phys. 96. doi:10.1063/1.461972.

De′ Nobili, M., Rojas, A., Abrami, M., Lapasin, R., Grassi, M., 2015. Structure characterisation by means of rheological and nmr experiments as a first necessary approach to study the l-(+)-ascorbic acid diffusion from pectin and pectin/alginate films to agar hydrogels that mimic food materials. J. Food Eng. 165. doi:10.1016/j.jfoodeng.2015.05.014.

Destrade, M., Saccomandi, G., Sgura, I., 2017. Methodical fitting for mathematical models of rubber-like materials. Proc. R. Soc. A: 473, 20160811. URL: https://royalsocietypublishing.org/doi/abs/10.1098/rspa.2016.0811, doi:10.1098/rspa.2016.0811, arXiv:https://royalsocietypublishing.org/doi/pdf/10.1098/rspa.2016.0811.

Dietmar, G., Thomas, S., 2011. Fracture Mechanics - With an Introduction to Micromechanics. doi:10.1007/978-3-642-19240-1.

Djabourov, M., Clark, A.H., Rowlands, D.W., Ross-Murphy, S.B., 1989. Small-angle x-ray scattering characterization of agarose sols and gels. Macromolecules 22, 180–188. URL: https://doi.org/10.1021/ma00191a035, doi:10.1021/ma00191a035, arXiv:https://doi.org/10.1021/ma00191a035.

Donati, I., Paoletti, S., 2009. Material Properties of Alginates. Springer Berlin Heidelberg, Berlin, Heidelberg. pp. 1–53. URL: https://doi.org/10.1007/978-3-540-92679-5_1, doi:10.1007/978-3-540-92679-5_1.

Draget, K.I., Smidsr, O., Skjåk-Bræk, G., 2005. Alginates from Algae. American Cancer Society. URL: https://onlinelibrary.wiley.com/doi/abs/10.1002/3527600035.bpol6008, doi:10.1002/3527600035.bpol6008, arXiv:https://onlinelibrary.wiley.com/doi/pdf/10.1002/3527600035.bpol6008.

Edwards, S.F., Vilgis, T.A., 1988. The tube model theory of rubber elasticity. Rep. Progr. Phys. 51, 243–297. doi:10.1088/0034-4885/51/2/003.

Eichinger, B.E., 2015. Rubber elasticity: Solution of the james-guth model. Phys. Rev. E 91, 052601. URL: https://link.aps.org/doi/10.1103/PhysRevE.91.052601, doi:10.1103/PhysRevE.91.052601.

Elías-Zúñiga, A., 2006. A non-gaussian network model for rubber elasticity. Polymer 47, 907 – 914. doi:https://doi.org/10.1016/j.polymer.2005.11.078.

Elías-Zúñiga, A., Beatty, M.F., 2002. Constitutive equations for amended non-gaussian network models of rubber elasticity. Int. J. Eng. Sci. 40, 2265 – 2294. doi:https://doi.org/10.1016/S0020-7225(02)00140-4.

Erman, B., 2010. Advances in constraint theories of rubber-like elasticity of polymers. Curr. Opin. Solid State Mater. Sci. 14, 35–37. doi:10.1016/j.cossms.2009.08.003.

Erman, B., Flory, P.J., 1982a. Relationships between stress, strain, and molecular constitution of polymer networks. comparison of theory with experiments. Macromolecules 15, 806–811. doi:10.1021/ma00231a023.

Erman, B., Flory, P.J., 1982b. Relationships between stress, strain, and molecular constitution of polymer networks. comparison of theory with experiments. Macromolecules 15, 806–811. doi:10.1021/ma00231a023.

Fariña, J., Sineriz, F., Molina, O., Perotti, N., 2001. Isolation and physicochemical characterization of soluble scleroglucan from sclerotium rolfsii. rheological properties, molecular weight and conformational characteristics. Carbohydr. Polym. 44, 41–50. doi:10.1016/S0144-8617(00)00189-2.

Feller, W., 1991. An Introduction to Probability Theory and Its Applications. John Wiley, New York.

Fixman, M., Alben, R., 1973. Polymer conformational statistics. i. probability distribution. J. Chem. Phys. 58, 1553–1558. doi:10.1063/1.1679394.

Flory, P., 1953. Principles of Polymer Chemistry. Baker lectures 1948, Cornell University Press, Ithaca, New York, USA. URL: https://books.google.it/books?id=CQ0EbEkT5R0C.

Flory, P.J., Erman, B., 1982. Theory of elasticity of polymer networks. 3. Macromolecules 15, 800–806. doi:10.1021/ma00231a022.

Flory, P.J., Rehner, J., 1943a. Statistical mechanics of cross-linked polymer networks ii. swelling. J. Chem. Phys. 11, 521–526. doi:10.1063/1.1723792.

Flory, P.J., Rehner, J., 1943b. Statistical mechanics of cross-linked polymer networks ii. swelling. J. Chem. Phys. 11, 521–526. doi:10.1063/1.1723792.

Fox, M., 2001. Optical Properties of Solids. Oxford University Press, Oxford.

Gedde, U.W., 1995. Polymer Physics. Chapman & Hall, London.

de Gennes, P., 1979. Scaling Concepts in Polymer Physics. Cornell University Press, Ithaca, New York, USA.

Gent, A.N., 1996. A New Constitutive Relation for Rubber. Rubber Chem. Technol. 69, 59–61. URL: https://doi.org/10.5254/1.3538357, doi:10.5254/1.3538357, arXiv:https://meridian.allenpress.com/rct/article-pdf/69/1/59/1945987/1_3538357.pdf.

Gong, J., Katsuyama, Y., Kurokawa, T., Osada, Y., 2003. Double-network hydrogels with extremely high mechanical strength. Adv. Mater. 15, 1155–1158. doi:10.1002/adma.200304907.

Gottlieb, M., 1982. The relationship between the modified flory rubber elasticity theory and the dossin–graessley small strain model. J. Chem. Phys. 77, 4783–4785. doi:10.1063/1.444386.

Grassi, M., Lapasin, R., Coviello, T., Matricardi, P., Di Meo, C., Alhaique, F., 2009. Scleroglucan/borax/drug hydrogels: Structure characterisation by means of rheological and diffusion experiments. Carbohydr. Polym. 78, 377–383. doi:10.1016/j.carbpol.2009.04.025.

Grassi, M., Lapasin, R., Pricl, S., 1996. A study of the rheological behavior of scleroglucan weak gel systems. Carbohydr. Polym. 29, 169 – 181. URL: http://www.sciencedirect.com/science/article/pii/0144861795001204, doi:https://doi.org/10.1016/0144-8617(95)00120-4.

Gundogan, N., Okay, O., Oppermann, W.D.I., 2004. Swelling, elasticity and spatial inhomogeneity of poly(n,n-dimethylacrylamide) hydrogels formed at various polymer concentrations. Macrom. Chem. Phys. 205, 814–823. doi:10.1063/1.461972.

Hadizadeh, S., Linhananta, A., Plotkin, S.S., 2011. Improved measures for the shape of a disordered polymer to test a mean-field theory of collapse. Macromolecules 44, 6182–6197. doi:10.1021/ma200454e.

Hermans, J.J., 1962. Statistical thermodynamics of swollen polymer networks. J. Polym. Sci. 59, 191–208. URL: https://onlinelibrary.wiley.com/doi/abs/10.1002/pol.1962.1205916715, doi:10.1002/pol.1962.1205916715.

Hild, G., 1998. Model networks based on 'endlinking' processes: synthesis, structure and properties. Progr. Polym. Sci. 23, 1019 – 1149. doi:https://doi.org/10.1016/S0079-6700(97)00055-5.

Hill, J.M., Arrigo, D.J., 1995. New families of exact solutions for finitely deformed incompressible elastic materials. IMA J. Appl. Math. 54, 109–123. URL: https://doi.org/10.1093/imamat/54.2.109, doi:10.1093/imamat/54.2.109, arXiv:https://academic.oup.com/imamat/article-pdf/54/2/109/6765980/54-2-109.pdf.

Holz, M., Heil, S.R., Sacco, A., 2000. Temperature-dependent self-diffusion coefficients of water and six selected molecular liquids for calibration in accurate 1h nmr pfg measurements. Phys. Chem. Chem. Phys. 2, 4740–4742. URL: http://dx.doi.org/10.1039/B005319H, doi:10.1039/B005319H.

Hossain, M., Steinmann, P., 2013. More hyperelastic models for rubber-like materials: consistent tangent operators and comparative study. J. Mech. Behav. Mater. 22, 27–50. URL: https://doi.org/10.1515/jmbm-2012-0007, doi:10.1515/jmbm-2012-0007.

Huang, Y., Szleifer, I., Peppas, N.A., 2002. A molecular theory of polymer gels. Macromolecules 35, 1373–1380. doi:10.1021/ma011294r.

Huang, Z.P., 2014. A Novel Constitutive Formulation for Rubberlike Materials in Thermoelasticity. J. Appl. Mech. 81. URL: https://doi.org/10.1115/1.4025272, doi:10.1115/1.4025272. 041013.

Ilienko, A., 2013. Continuous counterparts of poisson and binomial distributions and their properties. Annales Univ. Sci. Budapest., Sec. Comp. 39, 1.

James, H.M., Guth, E., 1943. Theory of the elastic properties of rubber. J. Chem. Phys. 11, 455–481. doi:10.1063/1.1723785.

Johner, A., Vilgis, T.A., Joanny, J.F., . Polyelectrolyte gel elasticity in poor solvent. Macromol. Symp. 146, 223–226. doi:10.1002/masy.

19991460130.

Koetting, M.C., Peters, J.T., Steichen, S.D., Peppas, N.A., 2015. Stimulus-responsive hydrogels: Theory, modern advances, and applications. Materials Science and Engineering: R: Reports 93, 1 – 49. URL: http://www.sciencedirect.com/science/article/pii/S0927796X15000339, doi:https://doi.org/10.1016/j.mser.2015.04.001.

Kolmogorov, A.L., 1933. Sulla determinazione empirica di una legge di distribuzione. G. Ist. Ital. Attuari 4, 83–91. URL: https://ci.nii.ac.jp/naid/10030673552/en/.

Kotz, S., Kozubowski, T., Podgorski, K., 2001. The Laplace Distribution and Generalizations. A revisit with applications to communications, economics, engineering, and finance. Birkhäuser Boston, Inc., Boston, MA. doi:10.1007/978-1-4612-0173-1_5.

Kouwijzer, M., Pérez, S., 1998. Molecular modeling of agarose helices, leading to the prediction of crystalline allomorphs. Biopolymers 46, 11–29. doi:10.1002/(SICI)1097-0282(199807)46:1<11::AID-BIP2>3.0.CO;2-0.

Labropoulos, K., Niesz, D., Danforth, S., Kevrekidis, P., 2002. Dynamic rheology of agar gels: Theory and experiments. part i. development of a rheological model. Carbohydr. Polym. 50, 393–406. doi:10.1016/S0144-8617(02)00084-X.

Lapasin, R., Pricl, S., 1995. Rheology of Industrial Polysaccharides: Theory and Applications; Blackie Academic Professional. doi:10.1007/978-1-4615-2185-3.

Mark, J.E., 1992. Molecular aspects of rubberlike elasticity. Angew. Makromol. Chem. 202, 1–30. doi:10.1002/apmc.1992.052020101.

Mark, J.E., Curro, J.G., 1983. A non-gaussian theory of rubberlike elasticity based on rotational isomeric state simulations of network chain configurations. i. polyethylene and polydimethylsiloxane short-chain unimodal networks. J. Chem. Phys. 79, 5705–5709. doi:10.1063/1.445656.

Matricardi, P., Alhaique, F., Coviello, T., E., 2016. Polysaccahride Hydrogels: Characterization and Biomedical Applications. CRC Press, Taylor & Francis Group, Boca Raton, USA.

Matricardi, P., Meo, C.D., Coviello, T., Hennink, W.E., Alhaique, F., 2013. Interpenetrating polymer networks polysaccharide hydrogels for drug delivery and tissue engineering. Adv. Drug Deliv. Rev. 65, 1172 – 1187. URL: http://www.sciencedirect.com/science/article/pii/S0169409X13000628, doi:https://doi.org/10.1016/j.addr.2013.04.002.

Matricardi, P., Onorati, I., Coviello, T., Alhaique, F., 2006. Drug delivery matrices based on scleroglucan/alginate/borax gels. Int. J. Pharm. 316, 21–8. doi:10.1016/j.ijpharm.2006.02.024.

Meiboom, S., Gill, D., 1958. Modified spin-echo method for measuring nuclear relaxation times. Rev. Sci. Instrum. 29, 688–691. URL: https://doi.org/10.1063/1.1716296, doi:10.1063/1.1716296, arXiv:https://doi.org/10.1063/1.1716296.

Menduina, C., Freire, J.J., Llorente, M.A., Vilgis, T., 1986. Correctly averaged non-gaussian theory of rubberlike elasticity. application to the description of the behavior of poly(dimethylsiloxane) bimodal networks. Macromolecules 19, 1212–1217. doi:10.1021/ma00158a045.

Mergell, B., Everaers, R., 2001. Tube models for rubberelastic systems. Macromolecules 34, 5675–5686. doi:10.1021/ma002228c.

Mezzasalma, S.A., 2001. Polymer chain size from geodesic path and geometrical bolyai–lobachevskij partition function. application to swelling of macromolecules in solution and micellar growth. J. Stat. Phys. 102, 1331–1341. doi:10.1023/A:1004848630492.

Mezzasalma, S.A., 2008. Macromolecules in Solution and Brownian Relativity. Academic Press-Elsevier, London. doi:https://doi.org/10.1016/S1573-4285(07)00009-9.

Mihai, L.A., Goriely, A., 2017. How to characterize a nonlinear elastic material? a review on nonlinear constitutive parameters in isotropic finite elasticity. Proc. R. Soc. A 473, 20170607. URL: https://royalsocietypublishing.org/doi/abs/10.1098/rspa.2017.0607, doi:10.1098/rspa.2017.0607, arXiv:https://royalsocietypublishing.org/doi/pdf/10.1098/rspa.2017.0607.

Mihai, L.A., Woolley, T.E., Goriely, A., 2019. Likely equilibria of the stochastic rivlin cube. Phil. Trans. R. Soc. A 377, 20180068. URL: https://royalsocietypublishing.org/doi/abs/10.1098/rsta.2018.0068, doi:10.1098/rsta.2018.0068, arXiv:https://royalsocietypublishing.org/doi/pdf/10.1098/rsta.2018.0068.

Mooney, M., 1940. A theory of large elastic deformation. J. Appl. Phys. 11, 582–592. URL: https://doi.org/10.1063/1.1712836, doi:10.1063/1.1712836, arXiv:https://doi.org/10.1063/1.1712836.

Ngai, K.L., Roland, C.M., 1994. Junction dynamics and the elasticity of networks. Macromolecules 27, 2454–2459. doi:10.1021/ma00087a014.

Ogden, R.W., Hill, R., 1972. Large deformation isotropic elasticity – on the correlation of theory and experiment for incompressible rubberlike solids. Proc. R. Soc. London A 326, 565–584. URL: https://royalsocietypublishing.org/doi/abs/10.1098/rspa.1972.0026, doi:10.1098/rspa.1972.0026, arXiv:https://royalsocietypublishing.org/doi/pdf/10.1098/rspa.1972.0026.

Okumura, D., Kondo, A., Ohno, N., 2016. Using two scaling exponents to describe the mechanical properties of swollen elastomers. J. Mech. Phys. Solids 90, 61–76. URL: https://www.sciencedirect.com/science/article/pii/S0022509615301290, doi:https://doi.org/10.1016/j.jmps.2016.02.017.

Ornstein, L.S., Zernike, F., 1914. Accidental deviations of density and opalescence at the critical point of a single substance. Proc. R. Neth. Acad. Arts Sci. 17, 793–806.

Palleschi, A., Bocchinfuso, G., Coviello, T., Alhaique, F., 2005a. Molecular dynamics investigations of the polysaccharide scleroglucan: first study on the triple helix structure. Carbohydr. Res. 340, 2154 – 2162. URL: http://www.sciencedirect.com/science/article/pii/S0008621505003137, doi:https://doi.org/10.1016/j.carres.2005.06.026.

Palleschi, A., Bocchinfuso, G., Coviello, T., Alhaique, F., 2005b. Molecular dynamics investigations of the polysaccharide scleroglucan: first study on the triple helix structure. Carbohydr. Res. 340, 2154 – 2162. URL: http://www.sciencedirect.com/science/article/pii/S0008621505003137, doi:https://doi.org/10.1016/j.carres.2005.06.026.

Panyukov, S., 1989. Topology fluctuations in polymer networks. J. Exp. Theor. Phys. Lett. 69, 342–353.

Panyukov, S., 1990. Scaling theory of high elasticity. J. Exp. Theor. Phys. 98, 668–680.

Panyukov, S., Rabin, Y., 1996. Statistical physics of polymer gels. Phys. Rep. 269, 1 – 131. doi:https://doi.org/10.1016/0370-1573(95)00068-2.

Pasut, E., Toffanin, R., Voinovich, D., Pedersini, C., Murano, E., Grassi, M., 2008. Mechanical and diffusive properties of homogeneous alginate gels in form of particles and cylinders. J. Biomed. Mater. Res. A 87A, 808–818. URL: https://onlinelibrary.wiley.com/doi/abs/10.

1002/jbm.a.31680, doi:10.1002/jbm.a.31680, arXiv:https://onlinelibrary.wiley.com/doi/pdf/10.1002/jbm.a.31680.

Peköz, E.A., Röllin, A., 2011. New rates for exponential approximation and the theorems of rényi and yaglom. Ann. Probab. 39, 587–608. doi:10.1214/10-AOP559.

Pence, T.J., Tsai, H., 2006. Swelling-induced cavitation of elastic spheres. Mathematics and Mechanics of Solids 11, 527–551. URL: https://doi.org/10.1177/1081286504046481, doi:10.1177/1081286504046481.

Priss, L.S., 1981. Molecular origin of constants in the theory of rubber-like elasticity considering network chains steric interaction. Pure Appl. Chem. 53, 1581 – 1596.

Provencher, S.W., 1982. A constrained regularization method for inverting data represented by linear algebraic or integral equations. Comput. Phys. Commun. 27, 213 – 227. URL: http://www.sciencedirect.com/science/article/pii/0010465582901734, doi:https://doi.org/10.1016/0010-4655(82)90173-4.

Puglisi, G., Saccomandi, G., 2016. Multi-scale modelling of rubber-like materials and soft tissues: an appraisal. Proc. R. Soc. A 472, 20160060. URL: https://royalsocietypublishing.org/doi/abs/10.1098/rspa.2016.0060, doi:10.1098/rspa.2016.0060, arXiv:https://royalsocietypublishing.org/doi/pdf/10.1098/rspa.2016.0060.

R.C., B., M., D., S.F., E., M., W., 1981. Rubber-like elasticity. Polymer 22, 1010.

Richbourg, N.R., Peppas, N.A., 2020. The swollen polymer network hypothesis: Quantitative models of hydrogel swelling, stiffness, and solute transport. Progr. Polym. Sci. 105, 101243. URL: https://www.sciencedirect.com/science/article/pii/S0079670020300368, doi:10.1016/j.progpolymsci.2020.101243.

Rinaudo, M., Vincendon, M., 1982. 13c nmr structural investigation of scleroglucan. Carbohydr. Polym. 2, 135 – 144. URL: http://www.sciencedirect.com/science/article/pii/0144861782900595, doi:https://doi.org/10.1016/0144-8617(82)90059-5.

Ronca, G., Allegra, G., 1975. An approach to rubber elasticity with internal constraints. J. Chem. Phys. 63, 4990–4997. doi:10.1063/1.431245.

Rubinstein, M., Colby, R., 2003. Polymer Physics. Oxford University Press. URL: https://books.google.it/books?id=EJrYoAEACAAJ.

Rubinstein, M., Panyukov, S., 2002. Elasticity of polymer networks. Macromolecules 35, 6670–6686. doi:10.1021/ma0203849.

Saalwächter, K., Sommer, J.U., 2007. Nmr reveals non-distributed and uniform character of network chain dynamics. Macromol. Rapid Commun. 28, 1455–1465. URL: https://onlinelibrary.wiley.com/doi/abs/10.1002/marc.200700169, doi:10.1002/marc.200700169.

Scherer, G.W., 1994. Hydraulic radius and mesh size of gels. J. Sol-Gel Sci. Techn. 1, 285–291. URL: https://doi.org/10.1007/BF00486171, doi:10.1007/BF00486171.

Schurz, J., 1991. Rheology of polymer solutions of the network type. Progr. Polym. Sci. 16, 1 – 53. URL: http://www.sciencedirect.com/science/article/pii/0079670091900067, doi:https://doi.org/10.1016/0079-6700(91)90006-7.

Smirnov, N., 1948. Table for estimating the goodness of fit of empirical distributions. Ann. Math. Statist. 19, 279–281. URL: https://doi.org/10.1214/aoms/1177730256, doi:10.1214/aoms/1177730256.

Sommer, J., Vilgis, T.A., Heinrich, G., 1994. Fractal properties and swelling behavior of polymer networks. J. Chem. Phys. 100, 9181–9191. doi:10.1063/1.466673.

Sommer, J. -U., Saalwächter, K., 2005. Segmental order in end-linked polymer networks: A monte carlo study. Eur. Phys. J. E 18, 167–182. doi:10.1140/epje/i2005-10037-3.

Spencer, A., 1971. Theory of invariants, in: Eringen, A.C. (Ed.), Continuum Physics. Academic Press, New York, pp. 239–353. URL: https://www.sciencedirect.com/science/article/pii/B978012240801450008X, doi:https://doi.org/10.1016/B978-0-12-240801-4.50008-X.

Thorne, A., 1988. Spectroscophysics. Chapman and Hall Ltd, London.

Toda, A., 2011. Weak limit of the geometric sum of independent but not identically distributed random variables. ArXiv:1111.1786 , 1–13.

Treloar, L.R.G., 1973. The elasticity and related properties of rubbers. Rep. Progr. Phys. 36, 755–826. doi:10.1088/0034-4885/36/7/001.

Treloar, L.R.G., 1975. The Physics of Rubber Elasticity. 3rd ed. ed., Clarendon Oxford.

Usatenko, Z., Sommer, J.U., 2008. Calculation of the segmental order parameter for a polymer chain in good solvent. Macromol. Theory Simul. 17, 39–44. doi:10.1002/mats.200700053.

Valentín, J.L., Carretero-González, J., Mora-Barrantes, I., Chassé, W., Saalwächter, K., 2008. Uncertainties in the determination of cross-link density by equilibrium swelling experiments in natural rubber. Macromolecules 41, 4717–4729. doi:10.1021/ma8005087.

Varga, O., 1966. Stress-strain behavior of elastic materials: selected problems of large deformations. Polymer reviews, Interscience Publishers. URL: https://books.google.it/books?id=w7l-zQEACAAJ.

Vilgis, T., Wilder, J., 1998. Polyelectrolyte networks: elasticity, swelling, and the violation of the flory-rehner hypothesis. Comput. Theor. Poly. Sci. 8, 61 – 73. doi:https://doi.org/10.1016/S1089-3156(98)00015-4.

Viñarta, S.C., François, N.J., Daraio, M.E., Figueroa, L.I., Fariña, J.I., 2007. Sclerotium rolfsii scleroglucan: The promising behavior of a natural polysaccharide as a drug delivery vehicle, suspension stabilizer and emulsifier. Int. J. Biol. Macromol. 41, 314 – 323. URL: http://www.sciencedirect.com/science/article/pii/S0141813007001043, doi:https://doi.org/10.1016/j.ijbiomac.2007.04.001.

de Vos, P., Bučko, M., Gemeiner, P., Navrátil, M., Švitel, J., Faas, M., Strand, B.L., Skjak-Braek, G., Morch, Y.A., Vikartovská, A., Lacík, I., Kolláriková, G., Orive, G., Poncelet, D., Pedraz, J.L., Ansorge-Schumacher, M.B., 2009. Multiscale requirements for bioencapsulation in medicine and biotechnology. Biomaterials 30, 2559 – 2570. URL: http://www.sciencedirect.com/science/article/pii/S0142961209000210, doi:https://doi.org/10.1016/j.biomaterials.2009.01.014.

Wang, X., Ni, Q., 2003. Determination of cortical bone porosity and pore size distribution using a low field pulsed nmr approach. J. Orthop. Res. 21, 312–319. doi:10.1016/S0736-0266(02)00157-2.

Webber, R.E., Creton, C., Brown, H.R., Gong, J.P., 2007. Large strain hysteresis and mullins effect of tough double-network hydrogels. Macromolecules 40, 2919–2927. doi:10.1021/ma062924y.

Whittall, K.P., MacKay, A.L., 1989. Quantitative interpretation of nmr relaxation data. J.Magn. Reson. 84, 134 – 152. URL: http://www.sciencedirect.com/science/article/pii/0022236489900115, doi:https://doi.org/10.1016/0022-2364(89)90011-5.

Wilber, J.P., Criscione, J.C., 2005. The baker–ericksen inequalities for hyperelastic models using a novel set of invariants of hencky strain. Int.

J. Solids Struct. 42, 1547–1559. URL: https://www.sciencedirect.com/science/article/pii/S0020768304004482, doi:10.1016/j.ijsolstr.2004.08.001.

Wu, P., van der Giessen, E., 1992. On improved 3-d non-gaussian network models for rubber elasticity. Mech. Res. Comm. 19, 427–433. URL: https://www.sciencedirect.com/science/article/pii/0093641392900212, doi:10.1016/0093-6413(92)90021-2.

7.1. Competing Interests

Authors declare no competing interests.

Appendices

7.2. Appendix A

We collect here the calculations of $\ln \Omega_{_1}$ for three end-to-end probability functions, $W(\mathbf{r})$, including their contributions to the mechanical quantities of interest (shear stress τ and elastic modulus G). They are carried out in accordance with Eqs. (15-16) of the theoretical section (Configuration Term).

I. *Laplace's density*. It is characterized by an exponential distribution of the form:

$$W_{_{iL}}(x_i) \;=\; \tfrac{1}{2} L_i \mathrm{e}^{-L_i|x_i|} \tag{A.1}$$

where L_i are normalization coefficients, playing the role of materials parameters. As it turns out:

$$\mathrm{I}_{_{iL}} + \mathrm{c}_{_{iL}} == -\alpha_i + 1\,, \tag{A.2}$$

Eq. (15) returns the Jacobian trace variation induced by the geometric transform:

$$\int_{\mathfrak{R}^3} W_{_L}(\mathbf{R}) \ln \frac{W_{_L}(\mathbf{r})}{W_{_L}(\mathbf{R})}\, d\mathbf{R} \;=\; 3 \;-\; \sum_i \alpha_i \tag{A.3}$$

implying:

$$\tfrac{1}{\nu} \ln \Omega_{_{1L}} = -(\alpha_x + \alpha_y + \alpha_z) + \ln(\alpha_x \alpha_y \alpha_z) + 3 \tag{A.4}$$

II. *Cauchy's density*. For Cauchy's distributions like:

$$W_{_{iC}}(x_i) \;=\; \frac{\chi_i}{\pi\left(x_i^2 + \chi_i^2\right)} \tag{A.5}$$

one gets instead:

$$\mathrm{I}_{_{iC}} + \mathrm{c}_{_{iC}} = -\ln(1+\alpha_i)^2 + 2\ln 2 \tag{A.6}$$

and:

$$\tfrac{1}{\nu} \ln \Omega_{_{1C}} = -\ln(1+\alpha_x)^2 - \ln(1+\alpha_y)^2 - \ln(1+\alpha_z)^2 + \ln(\alpha_x \alpha_y \alpha_z) + 6\ln 2 \tag{A.7}$$

where, again, the intrinsic materials parameters (χ_i) do not play any role here. We remind, despite a resemblance to normal distributions, Cauchy's densities have no moment-generating function (i.e. due to their heavy tails, average value and variance are also undefined).

III. *Poisson's density (continuous)*. Following some technical literature on this subject (see Ilienko (2013) in the main text) consider the probability distribution:

$$F_i^{(+)}(x_i) \;\equiv\; \begin{cases} 0 & x_i < 0 \\ f_i(x_i) & x_i \geq 0 \end{cases} \tag{A.8}$$

with:

$$f_i(x_i) \equiv \frac{\Gamma(x_i,\lambda_i)}{\Gamma(x_i)} \ , \tag{A.9}$$

where:

$$\Gamma(x_i) = \int_0^\infty t^{x_i-1}\mathrm{e}^{-t}dt \tag{A.10}$$

$$\Gamma(x_i,\lambda_i) = \int_{\lambda_i}^\infty t^{x_i-1}\mathrm{e}^{-t}dt \tag{A.11}$$

are, respectively, gamma and incomplete gamma functions, depending on a parameter $\lambda_i > 0$. Eq. (A.8) was introduced to define a continuous analogue of classical Poisson's law for non-negative values of the random variable, $F_i^{(+)}(x_i) = P\{\mathbf{x}_i \le x_i\}$. To extend it to the whole real axis, let us introduce:

$$F_i(x_i) = \tfrac{1}{2}\left[1 + F_i^{(+)}(x_i) + F_i^{(-)}(x_i)\right] \tag{A.12}$$

the odd counterpart being provided by:

$$F_i^{(-)}(x_i) \equiv - F_i^{(+)}(-x_i) \ . \tag{A.13}$$

Accordingly $F_i(0) = \frac{1}{2}$, and:

$$W_i(x_i) \equiv \tfrac{1}{2}\begin{cases} f_i'(-x_i) & x_i < 0 \\ f_i'(x_i) & x_i \ge 0 \end{cases} \tag{A.14}$$

is the Poisson density function to be used in Flory's configuration calculus. To improve its suitability for calculation purposes, observe that:

$$\left\{\frac{\Gamma(x_i,\lambda_i)}{\Gamma(x_i)}\right\}' = -\left\{\frac{\gamma(x_i,\lambda_i)}{\Gamma(x_i)}\right\}' \tag{A.15}$$

prime denoting differentiation with respect to the independent variable (x_i), while:

$$\gamma(x_i,\lambda_i) \equiv \int_0^{\lambda_i} t^{x_i-1}\mathrm{e}^{-t}dt = \Gamma(x_i) - \Gamma(x_i,\lambda_i) \tag{A.16}$$

We now recall two theorems about Gamma-like functions:

$$\Gamma(x_i) = \frac{\mathrm{e}^{-\ell x_i}}{x_i}\prod_{k=1}^\infty \frac{\mathrm{e}^{\frac{x_i}{k}}}{1+\frac{x_i}{k}} \tag{A.17}$$

$$\gamma(x_i,\lambda_i) = \frac{\lambda_i^{x_i}}{x_i}\Phi(1,1+x_i;\lambda_i) \ , \tag{A.18}$$

$\ell \approx 0.577$ being Euler's constant and Φ standing for a confluent hypergeometric function:

$$\Phi(1,1+x_i;\lambda_i) = 1 + \frac{\lambda_i}{1+x_i} + \frac{\lambda_i^2}{(1+x_i)(2+x_i)} + \ ... \tag{A.19}$$

and rearrange Eqs. (A.14-A.15) so to get:

$$W_{iP}(x_i) = -\tfrac{1}{2}\,\mathrm{e}^{-\lambda_i}A_1A_2A_3\left[\ell + (\ln A_2)' + (\ln A_3)'\right] \tag{A.20}$$

with:

$$A_1 = e^{\ell x_i}, \quad A_2 = \prod_{k=1}^{\infty} e^{-\frac{x_i}{k}} \left(1 + \frac{x_i}{k}\right), \quad A_3 = \lambda^{x_i} \Phi(1, 1 + x_i; \lambda_i) \tag{A.21}$$

After some developments, the second term in the square parenthesis becomes:

$$(\ln A_2)' = -x_i \sum_{k=1}^{\infty} \frac{1}{k(k + x_i)} \tag{A.22}$$

being:

$$\sum_{k=1}^{\infty} \frac{1}{k(k + x_i)} = \frac{1}{x_i} \int_0^1 \frac{1 - t^{x_i}}{1 - t} dt = \frac{1}{x_i} \left[\psi(x_i + 1) - \psi(1)\right], \tag{A.23}$$

in which:

$$\psi(z) \equiv [\ln \Gamma(z)]' = \psi(1 + z) - \frac{1}{z} \tag{A.24}$$

is the digamma function, and:

$$(\ln A_2)' = -\left[\psi(x_i) + \frac{1}{x_i} + \ell\right]. \tag{A.25}$$

A_3 can be rewritten by a direct evaluation of the derivative Φ', getting:

$$(\ln A_3)' = \ln \lambda_i - \frac{\lambda_i e^{\lambda_i}}{(1 + x_i)^2} \frac{\widehat{\Phi}}{\Phi} \tag{A.26}$$

where, again, $\Phi = \Phi(1, 1 + x_i; \lambda_i)$, while the hypergeometric series at the numerator reads $\widehat{\Phi} = \widehat{\Phi}(1 + x_i, 1 + x_i; 2 + x_i, 2 + x_i; -\lambda_i)$, i.e.:

$$\widehat{\Phi} = 1 + \frac{(1 + x_i)^2}{(2 + x_i)^2} \frac{(-\lambda_i)}{1!} + \frac{(1 + x_i)^2}{(3 + x_i)^2} \frac{(-\lambda_i)^2}{2!} + \ldots . \tag{A.27}$$

Finally, by gathering all calculations and taking into account that W_i is an even function, the configuration calculus can be carried out in terms of $\widetilde{W}_{iP} = 2W_{iP}$ over the only positive axis:

$$\widetilde{W}_{iP}(x_i) = \frac{\gamma(x_i, \lambda_i)}{\Gamma(x_i)} \left\{\psi(x_i + 1) + \frac{\lambda_i e^{\lambda_i}}{(1 + x_i)^2} \frac{\widehat{\Phi}}{\Phi} - \ln \lambda_i\right\} \tag{A.28}$$

7.3. Appendix B

Since Eq. (A.28) is too complicated to get a closed-form result in Flory's calculus, we concentrate hereinafter on its exponential regime, pointed out by small parameter values, $\lambda_i \ll 1$ (or, in the strongest sense, $\lambda \to 0^+$). Whenever possible in the next calculations indices i will be omitted.
A first point to make is that, as γ, Φ and $\widehat{\Phi}$ are all power series of λ, then when $\lambda \ll 1$:

$$\gamma(t, \lambda) = \sum_{n=0}^{\infty} (-1)^n \frac{\lambda^{n+t}}{n!(n + t)} \approx \frac{\lambda^t}{t}, \tag{B.1}$$

$$\lambda \frac{\Phi}{\widehat{\Phi}} \to 0 \tag{B.2}$$

and, neglecting ψ in comparison to $|\ln\lambda|$, one is left with:

$$\widetilde{W}_{_P}(t) \;\approx\; -\,\frac{\lambda^t \ln\lambda}{t\Gamma(t)} \tag{B.3}$$

The contributions to Flory's integral, which only matter to the mechanical responses, become:

$$(\ln\lambda)^{-1}\mathrm{I}\,(\alpha) \;\approx\; -(\ln\lambda)\,\alpha\,\Xi_\lambda[1] \;+\; (\ln\alpha)\,\Xi_\lambda\left[t^{-1}\right] \;+\; \Xi_\lambda\left[t^{-1}\ln\Gamma(\alpha t)\right] \;+\; \text{const.} \tag{B.4}$$

in which the functional notation in Eq. (23) was employed. Now:

$$\frac{1}{\Gamma(z+1)} \;=\; \sum_{k=0}^{\infty}\beta_k z^k \tag{B.5}$$

so that:

$$\beta_{n+1} = \;(n+1)^{-1}\sum_{j=0}^{n}(-1)^j s_{j+1}\beta_{n-j}\;, \tag{B.6}$$

with $\beta_{_0}=1$, while the coefficients:

$$s_j \;=\; \begin{cases} \ell & j=1 \\ \zeta(j) & j>1 \end{cases} \tag{B.7}$$

depend on Riemann's zeta function $\zeta(j)$. Since:

$$\Gamma(z+1) \;=\; z\Gamma(z)\;, \tag{B.8}$$

one obtains:

$$\Xi_\lambda\,[1] \;=\; \sum_{k=0}^{\infty}\beta_k\Lambda_{k+1} \tag{B.9}$$

in which, still for notational simplicity, we have set:

$$\Lambda_n \equiv \;\int_0^\infty \lambda^t t^n dt \;=\; (-1)^{1+n}\frac{\Gamma(1+n)}{(\ln\lambda)^{1+n}} \;>\; 0 \tag{B.10}$$

Thus, as:

$$-\,\alpha(\ln\lambda)^2\sum_{k=0}^{\infty}(-1)^k\beta_k\frac{\Gamma(k+2)}{(\ln\lambda)^{k+2}} \;=\; -\alpha\left\{\beta_{_0}\Gamma(2)-\beta_{_1}\frac{\Gamma(3)}{\ln\lambda}+\;\ldots\;\right\}\;, \tag{B.11}$$

substituting $\Gamma(n)=(n-1)!$ and the values of β_k, the first-order contribution in $(\ln\lambda)^{-1}$ is:

$$-\,\alpha(\ln\lambda)^2\,\Xi_\lambda\,[1] \;=\; -\alpha\left(1-\frac{2\ell}{\ln\lambda}\right) \;+\; \mathrm{O}(2) \tag{B.12}$$

To go ahead, note that:

$$\Xi_\lambda\left[t^{-1}\right] \;=\; \sum_{k=0}^{\infty}(-1)^k\beta_k\Lambda_k \tag{B.13}$$

from which:

$$(\ln\lambda)(\ln\alpha)\,\Xi_\lambda\left[t^{-1}\right] \;=\; \left(-1+\frac{\ell}{\ln\lambda}\right)\ln\alpha \;+\; \mathrm{O}(2) \tag{B.14}$$

The last term in Eq. (B.4) rapidly converges in $t \in [0,1]$. From the expansion $\ln\Gamma(\alpha t) = -\ \ln(\beta_0 \alpha t + \beta_1 \alpha^2 t^2 \ ... \ )$:

$$\Xi_\lambda \left[t^{-1} \ln\Gamma(\alpha t)\right] \ \approx \ - \sum_{r=0}^{\infty} \beta_r \int_0^{\infty} \lambda^t t^r \ln(\beta_0 \alpha t) dt \tag{B.15}$$

its dominant terms behave as $\sim \ln\alpha$:

$$\int_0^{\infty} \lambda^t t^r \ln(\beta_0 \alpha t) dt \ = \ \frac{(-1)^r}{(\ln\lambda)^{r+1}} \left\{ r! \left[\ell + \ln(-\ln\lambda) - \ln(\beta_0 \alpha) \right] \ + \ \text{const.} \right\} \tag{B.16}$$

thus we don't expect it is playing a significant role in experiments on isotropic media held at constant volume. However, as it represents the main signature of this end-to-end statistics, we leave it at the moment as it is. In conclusion, from the expression:

$$\mathrm{I}_i(\alpha_i) \ \approx \ -(\alpha_i + \ln\alpha_i) \ + \ \frac{\ell}{\ln\lambda_i} \left(2\alpha_i + \ln\alpha_i\right) \ + \ (\ln\lambda_i)\, \Xi_{\lambda_i} \left[t^{-1} \ln\Gamma(\alpha_i t)\right] \ + \ \text{const.} \tag{B.17}$$

a 'ground state' approximation may be written as:

$$\tfrac{1}{\nu} \ln \Omega_{1P}^{(1)} \approx \ - \sum_i \alpha_i \ + \ \sum_k \Xi_{\lambda_k}^{(1)} \left[t^{-1} \ln\Gamma(\alpha_k t)\right] \ln\lambda_k \ + \ \text{const.} \tag{B.18}$$

while, at next order:

$$\tfrac{1}{\nu} \ln \Omega_{1P}^{(2)} \approx \ - \sum_i \alpha_i \ + \ \ell \sum_p \frac{2\alpha_p + \ln\alpha_p}{\ln\lambda_p} \ + \ \sum_k \Xi_{\lambda_k}^{(2)} \left[t^{-1} \ln\Gamma(\alpha_k t)\right] \ln\lambda_k \ + \ \text{const.} \tag{B.19}$$

Observe the Jacobian-logarithmic term in Flory's theory is replaced in Eqs. (B.18-B.19) by an integral of the logarithm of Γ, whereas the Jacobian trace is typical instead of exponential (e.g. Laplace's) statistics. Entropic constants are not available in these equation models.
As a last remark to be made, as $\widetilde{W}_p$ was tackled upon $\lambda_i \ll 1$, its normalization condition should be rediscussed. Nevertheless, a numerical check performed with $\lambda_i \lesssim 10^{-2}$ returned:

$$\int_0^{\infty} \widetilde{W}_p(t; \lambda_i \ll 1)\, dt \ = \ 1 + \varepsilon(\lambda_i) \tag{B.20}$$

with $\varepsilon \leq 5 \cdot 10^{-2}$, i.e. a reasonable agreement within a few percents.

7.4. Appendix C

We regard here the perfect gas term as a functional perturbed by polymer statistics. It relies on the analysis presented in the second theoretical subsection and, in particular, on Eq. (28):

$$p \ = \ \prod_i \int_{-\frac{\delta x_i}{2}}^{\frac{\delta x_i}{2}} W_i(u) du \tag{C.1}$$

which has to be Taylor-expanded in δx_i. In the Gaussian case, we factorize for convenience β:

$$W_n(\mathbf{r}; \beta) \ = \ \prod_i W_{in}(\mathbf{e}_i \cdot \mathbf{r}; \beta_i) \ , \ \ \beta^3 \ \equiv \ \prod_i \beta_i \tag{C.2}$$

obtaining:

$$p \ = \ \left(\frac{\beta}{\sqrt{\pi}}\right)^3 \left[1 - \tfrac{1}{2} \sum_i (\beta_i \delta x_i)^2\right] \delta V \ + \ \mathrm{O}(7) \tag{C.3}$$

so that $(\beta/\sqrt{\pi})^3\delta V$ identifies the probability P_n and the functional form to adopt is:

$$P_n \approx \frac{\delta v}{V}\left\{1-\frac{\pi}{12}\left[\left(\frac{\delta x}{x}\right)^2+\left(\frac{\delta y}{y}\right)^2+\left(\frac{\delta z}{z}\right)^2\right]\right\}^{-1} \tag{C.4}$$

As expected, the perturbation in square parenthesis formally resembles the dependence of $\ln\Omega_{1n}(\alpha_i)$, producing a correction factor in the new configuration partition function (Ω_{2N}):

$$\Omega_{2N} \approx \omega_{2n}\Omega_{2n} \tag{C.5}$$

which reads:

$$\tfrac{1}{\nu}\ln\omega_{2n} = -\tfrac{1}{2}\ln\left\{1-\frac{\pi}{12}\left[\alpha_x^{-2}\left(\frac{\delta x}{x_0}\right)^2+\alpha_y^{-2}\left(\frac{\delta y}{y_0}\right)^2+\alpha_z^{-2}\left(\frac{\delta z}{z_0}\right)^2\right]\right\} \tag{C.6}$$

and, finally:

$$\tfrac{1}{\nu}\ln\Omega_{2N} \approx \tfrac{1}{\nu}\ln\Omega_{2n}+\tfrac{\pi}{24}\,\xi_2\sum_i\alpha_i^{-2} \tag{C.7}$$

where Flory's $\ln\Omega_{2n}$ is still given by Eq. (27), while:

$$\xi_h \approx \tfrac{1}{3}\sum_i\left(\frac{\delta x_i}{x_{0i}}\right)^h \tag{C.8}$$

introduces an average length-scale parameter of order h, quantifying the coupling effect of network units to the mechanical response (at a scale $\sim x_{0i}$). For simplicity, multiplicative factors in each perturbation term are grouped onward into single coefficients (e.g. $\xi_n \equiv \frac{\pi}{24}\xi_2$).

I. *Laplace's density*. In this case:

$$\prod_i\left[\int_{-\frac{\delta x_i}{2}}^{0}W_{iL}(u<0)du+\int_0^{\frac{\delta x_i}{2}}W_{iL}(u>0)du\right]=(1-\tfrac{1}{4}\sum_k L_k\delta x_k)\prod_i\tfrac{1}{2}L_i\delta x_i+\mathrm{O}(5) \tag{C.9}$$

and, letting $P_L=\frac{1}{2}\prod_i L_i\delta x_i$, one gets again a perturbation form conforming to Eq. (52):

$$P_L \approx \frac{\delta v}{V}\left[1-\tfrac{1}{2}\left(\frac{\delta x}{x}+\frac{\delta y}{y}+\frac{\delta z}{z}\right)\right]^{-1} \tag{C.10}$$

With the same notations of Eq. (C.5):

$$\Omega_{2L} \approx \omega_{2L}\Omega_{2n} \tag{C.11}$$

the interlinking perturbation now writes:

$$\tfrac{1}{\nu}\ln\omega_{2L} \approx \tfrac{1}{4}\left[\alpha_x^{-1}\left(\frac{\delta x}{x_0}\right)+\alpha_y^{-1}\left(\frac{\delta y}{y_0}\right)+\alpha_z^{-1}\left(\frac{\delta z}{z_0}\right)\right] \tag{C.12}$$

yielding, with $\xi_L\equiv\frac{1}{4}\xi_1$:

$$\tfrac{1}{\nu}\ln\Omega_{2L} \approx \tfrac{1}{\nu}\ln\Omega_{2n}+\xi_L\sum_i\alpha_i^{-1} \tag{C.13}$$

II. *Cauchy's density*. Taylor's series at leading orders of Gaussian and Cauchy's distributions coincide upon $\chi_i \to \beta_i^{-1}$:

$$\prod_i \int_{-\frac{\delta x_i}{2}}^{\frac{\delta x_i}{2}} W_{iC}(u)du \;=\; \left[1 - \tfrac{1}{12}\sum_k \left(\frac{\delta x_k}{\chi_k}\right)^2\right] \prod_i \left(\frac{\delta x_i}{\sqrt{\pi}\chi_i}\right) + \;\mathrm{O}(5) \tag{C.14}$$

i.e.:

$$P_{_C} \;=\; P_{_n} \;+\; \mathrm{O}(5) \tag{C.15}$$

and, let $\xi_{_C} \equiv \frac{\pi}{24}\xi_{_2}$:

$$\tfrac{1}{\nu}\ln\Omega_{_{2C}} \approx\; \tfrac{1}{\nu}\ln\Omega_{_{2n}} \;+\; \xi_{_C}\sum_i \alpha_i^{-2} \tag{C.16}$$

III. *Poisson's density*. Near the exponential limit, Taylor's expansion resembles Eq. (C.9):

$$p \;=\; -\;\left[1 + \tfrac{1}{4}\sum_r l_r(\ln\lambda_r)\;\delta x_r\right] \prod_i \tfrac{1}{2}(\ln\lambda_i)\delta x_i \;+\; \mathrm{O}(5) \tag{C.17}$$

with the three semi-heuristic coefficients $l_i = 1 - \frac{2\ell}{\ln\lambda_i} > 1$. On identifying $P_{_P} = -\frac{1}{2}\prod_i(\ln\lambda_i)\delta x_i$, one obtains:

$$P_{_P} \approx\; \frac{\delta v}{V}\left[1 - \tfrac{1}{2}\left(l_x\frac{\delta x}{x} \;+\; l_y\frac{\delta y}{y} \;+\; l_z\frac{\delta z}{z}\right)\right]^{-1} \tag{C.18}$$

that, consistently with the exponential domain of Poisson's statistics, approaches $P_{_L}$ as $l_i \to 1^-$. Proceeding as usual with:

$$\Omega_{_{2P}} \approx\; \omega_{_{2P}}\Omega_{_{2n}} \tag{C.19}$$

it turns out:

$$\tfrac{1}{\nu}\ln\omega_{_{2P}} \approx\; \tfrac{1}{4}\left[l_x\alpha_x^{-1}\left(\frac{\delta x}{x_{_0}}\right) +\; l_y\alpha_y^{-1}\left(\frac{\delta y}{y_{_0}}\right) +\; l_z\alpha_z^{-1}\left(\frac{\delta z}{z_{_0}}\right)\right] \tag{C.20}$$

or:

$$\tfrac{1}{\nu}\ln\Omega_{_{2P}} \approx\; \tfrac{1}{\nu}\ln\Omega_{_{2n}} \;+\; \xi_{_P}\sum_i \alpha_i^{-1} \tag{C.21}$$

where, let:

$$\xi_{_1}^* \;=\; \tfrac{1}{3}\sum_i l_i\left(\frac{\delta x_i}{x_{_{0i}}}\right) \;\geq\; \xi_{_1} \tag{C.22}$$

the coupling coefficient in Eq. (C.21) reads $\xi_{_P} \equiv \frac{1}{4}\xi_{_1}^*$.

7.5. Appendix D

We infer here the effect of the first configuration integral on the exponential limit of Poisson's statistics, where the experimental behavior deviates from Laplace's by the perturbation Ξ in Eq. (23). For simplicity, calculations are specialized to unswollen networks for $\xi_{_L}, \xi_{_P} \to 0^+$, deducing the mechanical features of an isotropic system for $\mathrm{Q} \neq 1$, $\lambda \ll 1$.

In SH experiments, the lowest order displacement between the $\ln \Omega_{_1}$ contributions (subindices 1) to the shear stress in Poisson's and Laplace's statistics is given by:

$$\tau_{_{1,P}} - \tau_{_{1,L}} = -G_{_F}\left(\frac{\partial\gamma}{\partial\alpha}\right)^{-1}\sum_{\mathrm{D}_{_S}(\alpha_i,1)}\ln\lambda_i\left(\frac{\partial\Xi^{(1)}_{\lambda_i}\left[t^{-1}\ln\Gamma(\alpha_i t)\right]}{\partial\alpha}\right)_{T,V} \tag{D.1}$$

still comprising a sum at constant volume, to be constrained to $\mathrm{D}_{_S}(\alpha_i, 1)$ according to:

$$\left(\frac{\partial\Xi_{\lambda_i}\left[t^{-1}\ln\Gamma(\alpha_i t)\right]}{\partial\alpha}\right)_{T,V} \equiv \Xi_{\lambda_i}\left[\psi(\alpha_i t)\right] \tag{D.2}$$

We work it out by evaluating the expansion:

$$\psi(z+1) = -\ell + \sum_{\infty}^{k=2}(-1)^k\zeta(k)z^{k-1} \tag{D.3}$$

at $z = \alpha_i t$:

$$\Xi_{\lambda_i}\left[\psi(\alpha_i t)\right] = -\frac{1}{\alpha_i}\sum_{k=0}^{\infty}\beta_k\Lambda_k + \alpha_i\sum_{k=0}^{\infty}\beta_k\sum_{m=0}^{\infty}(-1)^m\zeta(m+2)\alpha_i^m\Lambda_{m+k+2} \tag{D.4}$$

and, since $\Lambda_r \approx \lambda^{-1-r}$, the leading term is:

$$\Xi_{\lambda_i}\left[\psi(\alpha_i t)\right] \approx (\alpha_i\ln\lambda_i)^{-1} \tag{D.5}$$

On the other hand, the derivative:

$$\left(\frac{\partial\Xi_{\lambda_i}\left[t^{-1}\ln\Gamma(\frac{t}{\alpha})\right]}{\partial\alpha}\right)_{T,V} = -\frac{1}{\alpha^2}\,\Xi_{\lambda_i}\left[\psi(\tfrac{t}{\alpha})\right] \tag{D.6}$$

cancels the perturbation in Eq. (D.1), i.e.:

$$\Xi^{(1)}_{\lambda_x}\left[\psi(\alpha t)\right]\ln\lambda_x = -\Xi^{(1)}_{\lambda_y}\left[\psi(\tfrac{t}{\alpha})\right]\ln\lambda_y \tag{D.7}$$

getting back to the lowest-order responses as predicted in Laplace's statistics:

$$\tau_{_{1,P}} = \tau_{_{1,L}}\,, \qquad G_{_{1,P}} = G_{_{1,L}} \qquad\qquad (\lambda_i \to 0^+) \tag{D.8}$$

At the subsequent order, the behavior is generally anisotropic, as it is affected by each λ_i:

$$\tfrac{1}{\nu}\ln\Omega^{(2)}_{_{1P}} \approx -\sum_r\alpha_r + \ell\sum_i\frac{2\alpha_i+\ln\alpha_i}{\ln\lambda_i} + \sum_p\Xi^{(2)}_{\lambda_p}\left[t^{-1}\ln\Gamma(\alpha_p t)\right]\ln\lambda_p + \text{const.} \tag{D.9}$$

i.e.:

$$\tau_{_{1,P}} \approx \tau_{_{1,L}} + \delta\tau_{_P} + \delta\tau_{\psi} \tag{D.10}$$

The first perturbation comes from:

$$\sum_{\mathrm{D}_{_S}(\alpha_i,1)}\frac{1}{\ln\lambda_i}\left(\frac{\partial}{\partial\alpha}\left[2\alpha_i + \ln\alpha_i\right]\right)_{T,V} = \frac{2}{\ln\lambda_x} + \left(\frac{1}{\ln\lambda_x} - \frac{1}{\ln\lambda_y}\right)\alpha^{-1} - \frac{2}{\ln\lambda_y}\alpha^{-2} \tag{D.11}$$

and reads:

$$\delta\tau_{_P} = -\frac{2\ell}{1+\alpha^2}\,G_{_F}\left[\frac{\alpha^2}{\ln\lambda_x} + \frac{\alpha}{2}\left(\frac{1}{\ln\lambda_x}-\frac{1}{\ln\lambda_y}\right) - \frac{1}{\ln\lambda_y}\right] \quad , \tag{D.12}$$

while the second follows from Eqs. (D.2-D.5):

$$\sum_{\mathrm{D}_{S^{(\alpha_i,1)}}} \Xi^{(2)}_{\lambda_i}\left[\psi(\alpha_i t)\right]\ln\lambda_i \;\approx\; \frac{1}{\alpha}\left(1-\frac{\ell}{\ln\lambda_x}\right) + \alpha\left(1-\frac{\ell}{\ln\lambda_y}\right)\left(-\frac{1}{\alpha^2}\right) \tag{D.13}$$

i.e.:

$$\delta\tau_{\psi} = \frac{\ell\alpha}{1+\alpha^2}\,G_{_F}\left[\left(\ln\lambda_x\right)^{-1} - \left(\ln\lambda_y\right)^{-1}\right] \tag{D.14}$$

To sum Eq. (D.12) to Eq. (D.14) cancels out $\delta\tau_{\psi}$, identifying the overall response:

$$\delta\tau_{_A} \equiv \delta\tau_{_P} + \delta\tau_{\psi} = \frac{2\ell}{1+\alpha^2}\,G_{_F}\left[\left(\ln\lambda_y\right)^{-1} - \alpha^2\left(\ln\lambda_x\right)^{-1}\right] \tag{D.15}$$

so that:

$$\tau_{_{1,P}} = \frac{\alpha}{\alpha^4-1}\left\{\alpha^2 - 1 + 2\ell\left[\left(\ln\lambda_x\right)^{-1} - \alpha^2\left(\ln\lambda_y\right)^{-1}\right]\right\}\gamma(\alpha)\,G_{_F} \tag{D.16}$$

and, for an isotropic medium ($\lambda_x=\lambda_y\equiv\lambda$, $l_{_P}\equiv 1-\frac{2\ell}{\ln\lambda}$) it turns out for $\lambda \ll 1$:

$$\tau_{_{1,P}} \approx l_{_P}\frac{\alpha^2-1}{\alpha^2+1}\,G_{_F} > \tau_{_{1,L}} \tag{D.17}$$

$$G_{_{1,P}} \approx l_{_P}\frac{\alpha}{\alpha^2+1}\,G_{_F} > G_{_{1,L}} \tag{D.18}$$

We have thus inferred that passing from Laplace's to Poisson's statistics in the unperturbed exponential limit ($\xi_{_L}$, $\xi_{_P}\to 0^+$, $\lambda \ll 1$) requires to multiply the shear mechanical properties by the factor $l_{_P}$. Perturbation effects then are additive in ξ_k, as it comes from Eqs. (52, 54).
Regarding the dependence on the swelling factor, consider the reduced configuration integral:

$$\mathrm{I}_{_{HP}} = \nu\sum_{\mathrm{D}_{S^{(\alpha_i,1)}}}\int_0^\infty \widetilde{W}_{_{iP}}(\lambda,t)\ln\widetilde{W}_{_{iP}}(\lambda,\alpha_i t)\,dt \tag{D.19}$$

and the corresponding shear modulus expression, near $\alpha\approx 1$:

$$G_{_{1,P}} \approx -\frac{k_{_B}T}{V_0\gamma}\left(\frac{\partial\ln\mathrm{I}_{_{HP}}}{\partial\gamma}\right)_{T,V} \tag{D.20}$$

i.e.:

$$G_{_{1,P}} \propto \int_0^\infty \frac{\lambda^t}{\Gamma(t)}\left[(t\psi(t)-1)\,\psi(t) - \frac{t\Gamma''(t)}{\Gamma(t)} + \ln\lambda\right]dt = \left\{\Xi\left[t\psi^2(t)\right] - \Xi\left[\psi(t)\right] - \Xi\left[t\psi(t)(\ln\Gamma(t))'\right] + (\ln\lambda)\,\Xi[1]\right\} \tag{D.21}$$

the proportionality constant, function of $G_{_F}$ and $\ln\lambda$, being unimportant to the present aim. The algebraic sum of the first three terms on the rightest side turns out to be negligible, and one is left with the only $\Xi[1]$ contribution. In fact:

$$\Xi\left[\psi(t)\right] \approx -\beta_0\Lambda_0 - \beta_1\Lambda_1 \tag{D.22}$$

$$\Xi\left[t\psi^2(t)\right] \approx \beta_0\Lambda_0 + \beta_1\Lambda_1 + 2\ell\beta_0\Lambda_1 \tag{D.23}$$

$$\Xi\left[t\psi(t)(\ln\Gamma(t))'\right] \approx 2(\beta_0\Lambda_0 + \beta_1\Lambda_1) + 2\ell\beta_0\Lambda_1 \tag{D.24}$$

and:

$$\Xi\left[t\psi^2(t)\right] - \Xi\left[\psi(t)\right] - \Xi\left[t\psi(t)(\ln\Gamma(t))'\right] = \mathrm{O}(3) \tag{D.25}$$

When $\mathrm{D}_S = \mathrm{D}_S(\alpha_i, \mathrm{Q} \neq 1)$, $\Xi[1]$ is linearly multiplied by $\mathrm{Q}^{\frac{1}{3}}\mathrm{Q}^{-1}$ (see Eq. B.4), rescaling Eq. (D.21) by means of $\mathrm{Q}^{-\frac{2}{3}}$, still in accordance with Eq. (73). The same factor will also rescale any value of ξ_L and ξ_P, in the presence of finite perturbations. By adopting an akin procedure, it can be equally shown that Laplace's and Poisson's uniaxial stresses and elastic moduli of unperturbed deformation experiments, $\mathrm{D}_U = \mathrm{D}_U(\alpha_i, \mathrm{Q} \neq 1)$, stand in the same proportionality relations, bringing to Eqs. (68-69) and Eqs. (72-73) of the main text.

7.6. Appendix E

Based on Fig. (2) and Table (1) of the main text, one can conclude that the number of cubical meshes (N_{TMi}) and sides (N_{TSi}) in the polymeric network at generation n_i are given, respectively, by:

$$\mathrm{N_{TMi}} = 1 + 26\sum_{\mathrm{k=1}}^{\mathrm{n_i}} 3^{3(\mathrm{k}-1)} \tag{E.1}$$

$$\mathrm{N_{TSi}} = 12 + 132\sum_{\mathrm{k=1}}^{\mathrm{n_i}} 3^{(\mathrm{k}-1)} \tag{E.2}$$

Considering that a real system is not composed by meshes of identical side ζ_i but, more realistically, comprises different meshes with sides spanning from ζ_1 to ζ_N, ($\zeta_1 < \zeta_2 < .. \ \zeta_i \ .. < \zeta_N$), we assume that the polymeric network is the result of summing up meshes of all dimensions. Thus, the fraction of meshes (F_{Mi}) and sides (F_{Si}) of length ζ_i is given by:

$$\mathrm{F_{Mi}} = \frac{1 + 26\sum_{\mathrm{k=1}}^{\mathrm{n_i}} 3^{3(\mathrm{k}-1)}}{\sum_{\mathrm{i=1}}^{\mathrm{N}}\left(1 + 26\sum_{\mathrm{k=1}}^{\mathrm{k=n_i}} 3^{3(\mathrm{k}-1)}\right)} \tag{E.3}$$

$$\mathrm{F_{Si}} = \frac{12 + 132\sum_{\mathrm{k=1}}^{\mathrm{n_1}} 3^{(\mathrm{k}-1)}}{\sum_{\mathrm{i=1}}^{\mathrm{N}}\left(1 + 132\sum_{\mathrm{k=1}}^{\mathrm{k=n_i}} 3^{(\mathrm{k}-1)}\right)} \tag{E.4}$$

In order to make the model more flexible, it is convenient moving from the discrete mesh (Eq. E.3) and side (Eq. E.4) distribution to a continuous one. Thus, differentiation of Eqs. (E.1) and (E.2) leads to:

$$\frac{\mathrm{dN_{TMi}}}{\mathrm{dk}} = 26{\cdot}3^{3(\mathrm{k}-1)}\ln_{\mathrm{e}}(3)\cdot 3 \tag{E.5}$$

$$\frac{\mathrm{dN_{TSi}}}{\mathrm{dk}} = 132{\cdot}3^{(\mathrm{k}-1)}\ln_{\mathrm{e}}(3) \tag{E.6}$$

while integrating Eq. (E.5) and (E.6) yields:

$$\mathrm{N_{TMi}} = \int \mathrm{dN_{TMi}} = 26{\cdot}\ln_{\mathrm{e}}(3){\cdot}3\int 3^{3(\mathrm{k}-1)}\mathrm{dk} = \frac{26}{27}3^{3(\mathrm{n_i}-1)} + \mathrm{C_M} \tag{E.7}$$

$$N_{TSi} = \int dN_{TSi} = 132 \cdot \ln_e(3) \int 3^{(k-1)} dk = \frac{132}{3} 3^{3n_i} + C_S \tag{E.8}$$

where C_M and C_S are two integration constants that follow from imposing that Eqs. (E.7) and (E.8) give the same estimation of N_{TMi} and N_{TSi}, as provided by Eqs. (E.1) and (E.2), respectively. Accordingly, we have:

$$\frac{26}{27} 3^{3(n_i-1)} + C_M = 1 + 26 \sum_{k=1}^{n_i} 3^{3(k-1)} \tag{E.9}$$

$$C_M = 1 + \frac{26}{27} \left(3^{3n_i} - 3^{3n_i}\right) + \frac{26}{27} \sum_{k=1}^{n_i-1} 3^{3k} = 1 + \frac{26}{27} \sum_{k=1}^{n_i-1} 3^{3k} \tag{E.10}$$

$$\frac{132}{3} 3^{3n_i} + C_S = 12 + 132 \sum_{k=1}^{n_i} 3^{(k-1)} \tag{E.11}$$

$$C_S = 12 + \frac{132}{3} \left(3^{n_i} - 3^{n_i}\right) + \frac{132}{3} \sum_{k=1}^{n_i-1} 3^k = 12 + \frac{132}{3} \sum_{k=1}^{n_i-1} 3^k \tag{E.12}$$

On the basis of Eqs. (E.10) and (E.12), Eqs.(E.7) and (E.8) become:

$$N_{TMi} = 1 + \frac{26}{27} 3^{3n_i} + \frac{26}{27} \sum_{k=1}^{n_i-1} 3^{3k} \tag{E.13}$$

$$N_{TSi} = 12 + \frac{132}{3} 3^{n_i} + \frac{132}{3} \sum_{k=1}^{n_i-1} 3^k \tag{E.14}$$

Assuming $n_i \geq 1$, it is easy to verify that the sum of the first and third term (summation) of Eq. (E.13) is negligible in comparison to the second one, so that:

$$N_{TMi} \approx \frac{26}{27} 3^{\,3n_i} \tag{E.15}$$

In Eq. (E.14), instead, prevailing terms are the second and first of the summation, thence:

$$N_{TSi}\% \approx \frac{132}{3}\, 3^{n_i} + \frac{132}{3}\, 3^{(n_i-1)} = 132 \cdot 3^{(n_i-1)} \left(1 + \frac{1}{3}\right) \tag{E.16}$$

and, in light of Eqs. (E.15) and (E.16), Eqs. (E.3) and (E.4) can be written as:

$$F_{Mi}\% \approx \frac{3^{3n_i}}{\sum_{i=1}^{N} 3^{n_i}} \tag{E.17}$$

$$F_{Si}\% \approx \frac{3^{n_i}}{\sum_{i=1}^{N} 3^{n_i}} \tag{E.18}$$

where now n_i are real numbers ≥ 1, whose determination comes from the experimental values of F_{Mi}, i.e. the probability P_i of finding a cubical mesh of size ζ_i (see Eq. 91):

$$\frac{P_2}{P_1} = \frac{F_{M2}}{F_{M1}} = 3^{3(n_2-n_1)}\,, \quad \frac{P_i}{P_{i-1}} = \frac{F_{Mi}}{F_{Mi-1}} = 3^{3(n_i-n_{i-1})} \tag{E.19}$$

Eq. (E19) allows to determine n_i in terms of n_1:

$$\mathrm{n_i} = \mathrm{n_{i-1}} + \frac{1}{3}\ln_3\left(\frac{\mathrm{P_i}}{\mathrm{P_{i-1}}}\right) = \mathrm{n_1} + \frac{1}{3}\ln_3\left(\frac{\mathrm{P_i}}{\mathrm{P_1}}\right) \tag{E.20}$$

and, finally, Eq. (E.20), Eq. (E.17) and Eq. (E.18) become:

$$\mathrm{F_{Mi}\%} \approx \frac{3^{3\mathrm{n_i}}}{\sum_{\mathrm{i=1}}^{\mathrm{N}} 3^{3\mathrm{n_i}}} = \frac{3^{3\left(\mathrm{n_1}+\frac{1}{3}\ln_3\left(\frac{\mathrm{P_i}}{\mathrm{P_1}}\right)\right)}}{\sum_{\mathrm{i=1}}^{\mathrm{N}} 3^{3\left(\mathrm{n_1}+\frac{1}{3}\ln_3\left(\frac{\mathrm{P_j}}{\mathrm{P_1}}\right)\right)}} = \frac{3^{\left(\ln_3\left(\frac{\mathrm{P_i}}{\mathrm{P_1}}\right)\right)}}{\sum_{\mathrm{i=1}}^{\mathrm{N}} 3^{\left(\ln_3\left(\frac{\mathrm{P_i}}{\mathrm{P_1}}\right)\right)}} = \frac{\mathrm{P_i}}{\sum_{\mathrm{i=1}}^{\mathrm{N}} \mathrm{P_i}} \tag{E.21}$$

$$\mathrm{F_{Si}\%} \approx \frac{3^{\mathrm{n_i}}}{\sum_{\mathrm{i=1}}^{\mathrm{N}} 3^{\mathrm{n_i}}} = \frac{3^{\left(\mathrm{n_1}+\frac{1}{3}\ln_3\left(\frac{\mathrm{P_i}}{\mathrm{P_1}}\right)\right)}}{\sum_{\mathrm{i=1}}^{\mathrm{N}} 3^{\left(\mathrm{n_1}+\frac{1}{3}\ln_3\left(\frac{\mathrm{P_j}}{\mathrm{P_1}}\right)\right)}} = \frac{3^{\left(\frac{1}{3}\ln_3\left(\frac{\mathrm{P_i}}{\mathrm{P_1}}\right)\right)}}{\sum_{\mathrm{i=1}}^{\mathrm{N}} 3^{\left(\frac{1}{3}\ln_3\left(\frac{\mathrm{P_i}}{\mathrm{P_1}}\right)\right)}} = \frac{\sqrt[3]{\mathrm{P_i}}}{\sum_{\mathrm{i=1}}^{\mathrm{N}} \sqrt[3]{\mathrm{P_i}}} \tag{E.22}$$